MASTER

On the influence of molecular doping on charge-carrier and exciton dynamics in polymer light-emitting diodes

van der Scheer, R.F.J.

Award date:
2002

On the Influence of Molecular Doping on Charge-Carrier and Exciton Dynamics in Polymer Light-Emitting Diodes

Master's Thesis

R.F.J. van der Scheer

June 2002

Supervisors:
prof. dr. M.A.J. Michels (Technische Universiteit Eindhoven)
dr. H. Brom (Universiteit Leiden)
dr. P.A. Bobbert (Technische Universiteit Eindhoven)
dr. K. Brunner (Philips Research Laboratories Eindhoven)

PFY

Technische Universiteit Eindhoven
Faculteit Technische Natuurkunde
Capaciteitsgroep Theoretische Polymeerfysica

Abstract

In this work the the dynamical properties of charge-carriers and excitons in polymer light-emitting diodes is researched.

The influence of molecular doping on the charge-carrier dynamics is studied by means of admittance spectroscopy. It appears that the interaction of the dopant with the electrons differs from the interaction of the dopant with the holes in the polymer. A shift of the compensation voltage of the PLED due to the doping is explained by a vacuum-level shift due to the interaction of the anode with the LUMO of the polymer.

Exciton dynamics is studied by means of Monte Carlo simulations. The motion of the excitons is described by the Förster process. The temperature dependence of the diffusivity of excitons in a constant density of states is explained by means of the Mott theory. The simulations of photoluminescence experiments predict a red shift of the average energy for increasing doping levels.

Acknowledgements

De volgende mensen wil ik bedanken voor hun bijdragen aan het werk dat u voor u ziet liggen:

Allereerst Thijs Michels voor de mogelijkheid om binnen de groep Theoretische Polymeerfysica af te studeren. Toen ik je ruim een jaar geleden om een afstudeerplaats vroeg waarin zowel experiment als theorie verwerkt zou zitten ben je gelijk aan de slag gegaan hetgeen resulteerde in een samenwerking met Philips en de universiteit van Leiden.

Hans Brom van het Kamerlingh Onnes laboratorium van de universiteit Leiden waar ik een paar maanden lang gastvrij ontvangen ben om metingen te verrichten samen met Iulian Hulea. Beide wil ik bedanken voor een leuke en leerzame periode waarin ik volledige experimentele vrijheid genoot.

Klemens Brunner van het Philips Natuurkundig Laboratorium wil ik bedanken voor samples en samenwerking. Vooral aan het einde van mijn project hebben we intensief samengewerkt, wat ik als zeer positief heb ervaren.

Peter Bobbert voor de begeleiding van het theoretische werk en menige discussie.

Stefan Meskers voor het belangeloos ter beschikking stellen van de code voor de Monte Carlo simulaties en vele vruchtbare discussies. Zonder die code had ik nooit zoveel kunnen doen als ik nu gedaan heb.

Frank, aan jou ben ik veel dank verschuldigd. Niet alleen vanwege de fijne samenwerking, maar vooral voor je goede begeleiding. Op het moment dat ik het afstuderen even niet meer zag zitten heb jij het op je genomen om me weer op gang te krijgen en zijn we samen aan de slag gegaan en hebben er iets moois van gemaakt, bedankt!

Paul van de Schoot voor je hulp met de theorie, maar bovenal voor goede gesprekken onder het genot van een goed glas wijn.

Raoul Trines voor hulp met LaTeX, Mathematica en voor algemene kennis.

Natuurlijk mijn medestudenten niet te vergeten: Jochen 'over de tafel' Schellekens, Mechiel 'C-Fix' Wilbrink, Lucas 'polsjes' Evers (de RvB), Joeri de Groot en Nazar Sushko. Mede dankzij jullie is mijn afstudeerperiode een onvergetelijke tijd geworden.

CONTENTS

CHAPTER 1

Introduction

Since the discovery of electroluminescence in conjugated polymers, understanding the processes underlying the emission of light in these devices is an important research effort, especially for optimizing the lifetime and efficiency of the polymers in the emissive layer. Recently these efforts have resulted in the realization of the first commercial products such as monochrome segmented and graphic displays. Though the broad spectrum of the emissive polymer in these products allows for a certain flexibility in the range of accessible colors by applications of filters, a true full color display cannot be achieved. The next step is a pixelated full color display. For this goal red, green and blue (RGB) colors have to be realized with good spectral purity. Besides the obvious route of applying three different polymers for the basic RGB colors there are several other approaches currently examined. One particular appealing solution is energy or charge transfer from a host polymer to emissive guest molecules, the so called dye molecules. This process can be optimized to high efficiencies already at low guest concentrations, which should leave the macroscopic properties of the polymer such as viscosity unchanged. This is particularly important for the efficient production of pixelated devices by ink jet printing because the printing proces has to be optimized for one ink instead of three.

In this report we study the influence of molecular doping using two different approaches. The first is by studying the dynamics of charge carriers in both doped and undoped polymer light-emitting diodes (PLEDs). The second approach is of theoretical nature and comprises Monte Carlo simulations of excitations in doped polymers.

1.1 PLEDs

A PLED consist of a thin layer of conjugated polymer sandwiched between a transparent indium-tin-oxide (ITO) electrode, the anode, and a BaAl electrode, the cathode. Conjugated polymers consist of alternating single and double bonds along the polymer chain (sp2-hybridised carbons). The π-electrons form a common π-electron system along the whole polymer chain. This π-electron system gives the polymers semiconducting properties. Since the work function of ITO lies close to the valence band or HOMO (highest occupied molecular orbital) of the polymer it serves well as a hole injector while preventing electron injection.

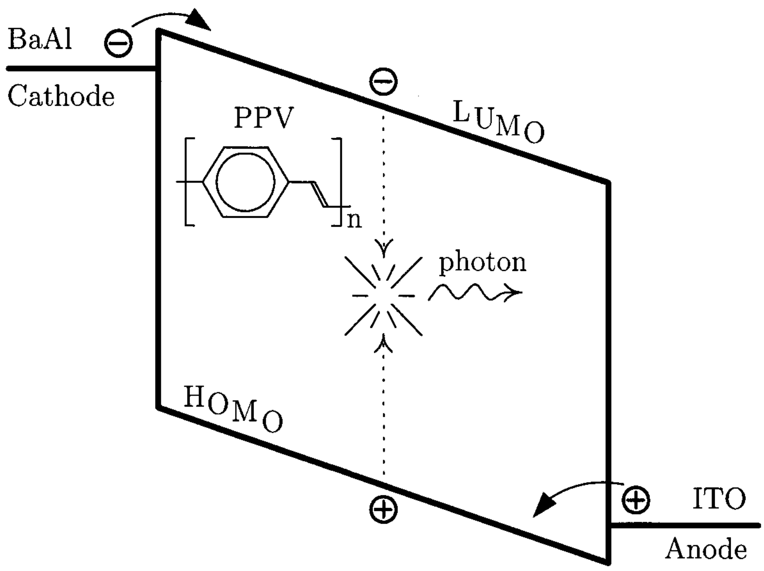

Figure 1.1: Energy-band diagram of a PLED in forward bias. Electrons and holes are injected into the polymer and transported under influence of the applied electric field until they recombine. When they recombine a photon is emitted.

The low work function of the BaAl cathode lies close to the conduction band or LUMO (lowest unoccupied molecular orbit) and serves as an electron injector. Operated in forward bias, as indicated in figure 1.1, electrons and holes are injected from the ITO and BaAl electrodes respectively. Under the influence of the applied electric field the carriers move through the polymer until they recombine under emission of a photon.

When a device has both a high-work function electrode (hole injector) and a low-work function electrode (electron injector) it is said to be a double-carrier (DC) device. If it has two high work function electrodes it is called a hole-only (HO) device since only holes can be injected into the device.

1.2 The Effect of Dye-doping on Charge Carrier Dynamics

By adding dye molecules to the polymer of a PLED the optical properties of the PLED are changed. The electrons and the holes are now supposed to recombine on the dye, emitting light corresponding to the energy gap of the dye. The recombination of charge-carriers in conjugated polymers has been shown to be of the Langevin type. This means that the recombination efficiency is limited by the diffusion of electrons and holes towards each other in their mutual Coulomb field, and therefore governed by the carrier mobility. Since both transport and recombination depend on the mobility it is of key importance to understand this parameter and to investigate the effect of the presence of dye molecules on the mobility. By studying properties such as the built-in potential (V_{bi}) and charge carrier mobility (μ) we hope to be able to draw general conclusions of how the operation of the PLED is changed by molecular doping and about the mechanism behind this change.

1.3 Exciton Transport in Polymers and the Effect of Dye-Doping

When an electron and a hole encounter each other in the active layer of a PLED they can recombine while emitting a photon. Another possibility is that they form a so-called exciton, a bound electron-hole pair. This exciton can move through the polymer like a single particle and has a an average lifetime (τ_{life}) after which it decays under emission of a photon. When an exciton is formed in the polymer it moves through the polymer via (dipole-dipole) Förster interaction. Two scenarios are now possible: either the exciton decays on the polymer and emits a photon corresponding to the energy gap of the polymer or it decays on a dye molecule and emits a photon corresponding to the energy gap of this molecule. The first option is for obvious reasons unfavorable. So the objective is to have as many excitons transported to the dye molecules as possible before they decay in the bulk.
The time scales which are important in the process of exciton transfer to the dye are:

- τ_{life}: the average lifetime of an exciton before it decays.
- τ_{relax}: the relaxation time. How long does it take for an ensemble of excitons, created at a certain energy, to reach thermal equilibrium
- $\tau_{pol \rightarrow dye}$: the average time needed for an exciton to reach a dye molecule.

In this work we want to investigate how efficient the exciton (Förster) transport from the polymer to the dye is. If, for example, $\tau_{pol \rightarrow dye} \gg \tau_{life}$ then most of the excitons will decay on the polymer and the efficiency will be low.

CHAPTER 2

Charge Carrier Mobility in PLEDs - Theory

Admittance spectroscopy has proved to be a powerful technique to investigate charge transport kinetics and relaxation. In this section a theoretical expression for the complex admittance, Y, of hole-only PPV devices as function of frequency is derived [MBP99]. The complex admittance Y is defined as the ratio of ac current and ac voltage:

$$Y = i_{ac}/v_{ac} = G + iB = G + i\omega C \tag{2.1}$$

with G the conductance, B the susceptance, C the capacitance and ω the angular frequency. This expression is used to fit the data obtained by admittance spectroscopy on a hole-only device. One of the parameters that is obtained from this fit is the hole mobility. It will be shown that it is possible to relate this mobility to certain relaxation effects in the admittance data and thereby obtaining a criterium for determining this mobility in a fairly simple and straightforward manner.

2.1 Frequency-Dependent Electrical Response of Holes

From previous studies it is known that the current in PPV PLEDs is space-charge limited [BV00], so v_{ac} directly modulates the number of charge carriers in the device. The timescale for the build-up of charge carriers is the transit time of the injected holes, τ_t. At low frequencies ($\omega < 1/\tau_t$) the built-up of space charge is fast enough to follow the modulation in v_{ac}, so the extra carriers lead to an additional current which lags behind the v_{ac}. The phase of Y decreases, resulting in an inductive (negative) contribution to the capacitance. For high frequencies ($\omega > 1/\tau_t$) the space charge cannot be redistributed in a period of the applied voltage and the measured capacitance is similar to the geometrical capacity, $C_0 = \varepsilon_0\varepsilon(\omega)A/L$. The frequency for which the space charge cannot be redistributed shifts to higher values for increasing bias, see figure 2.1.

For $V_{bias} = 0\text{V}$ no current injection takes place and the ac response is characteristic for an disordered insulator. The slow decrease of C with frequency reflects the relaxation of permanent dipoles present in the material. The disordered nature of the polymer material gives rise to a distribution of dipolar relaxation times. The dielectric response can be described by the empirical Cole-Cole euqation [BB85]:

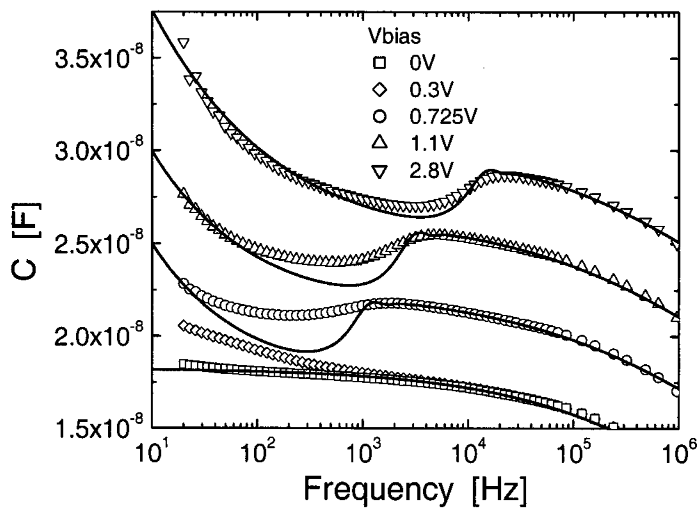

Figure 2.1: Frequency-dependent response of the capacitance of a hole-only device. The solid lines are fits to the SCLC model (2.11). The different data sets have an offset of 4nF for a better representation. The data of C, for $V_{bi} = 0.35V$, is also included (without offset).

$$\frac{\varepsilon(\omega)}{\varepsilon_0} = \varepsilon_\infty + \frac{\varepsilon_\infty - \varepsilon_s}{1 + (i\omega\tau_0)^{1-\beta}} \tag{2.2}$$

Fitting (2.2) to the data (figure 2.1) for $V_{bias} = 0$V gives $\varepsilon_s = 4.12$, $\varepsilon_\infty = 1.25$, $\tau_0 = 0.7 * 10^{-7}s$ and $\beta = 0.59$.

When the applied bias exceeds the built-in potential, the ac response of a biased PLED is described by the basic equations for time-dependent injection of space-charge limited current [LM70]. These are Poisson's equation in planar symmetry

$$\frac{\partial E(x,t)}{\partial x} = \frac{\rho(x,t)}{\varepsilon} \tag{2.3}$$

and the continuity equation

$$\frac{\partial \rho(x,t)}{\partial t} = -\frac{\partial i(x,t)}{\partial x}. \tag{2.4}$$

Using (2.3) in (2.4), we can derive the equation of the total current density:

$$J(t) = i(x,t) + \varepsilon\frac{\partial E(x,t)}{\partial t} \tag{2.5}$$

The steady-state and linear time-dependent contributions are are separated by introducing

$$E(x,t) = E_{dc}(x) + e_0(x)e^{i\omega_0 t}$$
$$\rho(x,t) = \rho_{dc}(x) + \rho_0(x)e^{i\omega_0 t}$$

$$J(t) = J_{dc} + j_0 e^{i\omega_0 t}$$
$$i(x,t) = i_{dc} + i_0(x) e^{i\omega_0 t}$$

Inserting these expressions into (2.3) and (2.5), linearizing the time-dependent contribution and using the linearized relation between current and electric field,

$$i_0(x) = q\mu(\omega_0)[\rho_{dc}(x)e_0(x) + \rho_0(x)E_{dc}(x)] = q\mu(\omega_0)[\rho_{dc}(x)e_0(x) + \varepsilon\frac{\partial e_0(x)}{\partial x}E_{dc}(x)] \tag{2.6}$$

we obtain

$$q\mu(\omega_0)\rho_{dc}(x)e_0(x) + \varepsilon\mu(\omega_0)E_{dc}(x)\frac{\partial e_0(x)}{\partial x} + i\varepsilon\omega_0 e_0(x) = j_0. \tag{2.7}$$

From [LM70] we know that for the steady state (space-charge limited) situation $\rho_{dc}(x) = \frac{3}{4}\frac{\varepsilon}{q}V\frac{1}{\sqrt{xL^3}}$, $E_{dc}(x) = \frac{3}{2}V\sqrt{\frac{x}{L^3}}$ and $\mu_{dc} = \frac{4}{3}\frac{L^2}{\tau V}$ (the latter comes from the time-of-flight-method). Now we can write (2.7) in the following way

$$p(\omega_0)x^{-\frac{1}{2}}e_0(x) + 2p(\omega_0)x^{\frac{1}{2}}\frac{\partial e_0(x)}{\partial x} + i\omega_0 e_0(x) = \frac{j_0}{\varepsilon} \tag{2.8}$$

with $p(\omega_0) = \frac{3}{4}VL^{-\frac{3}{2}}\mu(\omega_0) = L^{\frac{1}{2}}\tilde{\mu}(\omega_0)\tau^{-1}$, τ the transit time and $\tilde{\mu}(\omega_0) = \mu(\omega_0)/\mu_{dc}$ the normalized mobility. The solution of (2.8), with the ideal (ohmic) injecting contact modelled by the boundary condition $e_0(0) = 0$, is

$$e_0(x) = -\frac{j_0 p(\omega_0)}{\omega_0^2\varepsilon\sqrt{x}}\exp\left[-\frac{i\omega_0\sqrt{x}}{p(\omega_0)}\right] - \frac{i\omega_0 - \frac{p(\omega_0)}{\sqrt{x}}}{\omega_0^2\varepsilon}j_0 \tag{2.9}$$

By integrating this equation from anode to cathode we obtain for the potential

$$V = \int_0^L e_0(x)\mathrm{d}x = j_0\frac{2}{\omega^3\varepsilon}\left[ip(\omega_0)^2\left(1 - \exp\left[-\frac{i\omega_0\sqrt{L}}{p(\omega_0)}\right]\right) + \omega_0 p(\omega_0)\sqrt{L} - i\omega_0^2 L\right] \tag{2.10}$$

Finally, for the admittance we write [1]

$$Y = \frac{jA}{V} = \frac{\varepsilon A}{\tau L}\frac{\Omega^3}{2i\tilde{\mu}^2(\Omega)\left[1 - \exp\left(-\frac{-i\Omega}{\tilde{\mu}(\Omega)}\right)\right] + 2\Omega\tilde{\mu}(\Omega) - i\Omega^2} \tag{2.11}$$

with $\Omega = \omega_0\tau$ the normalized frequency.

For the frequency dependent mobility we use the following expression which follows from the dispersive nature of the charge transport [MBP99] [BB85]

$$\tilde{\mu}(\Omega) = 1 + M(i\Omega)^{1-\alpha} \tag{2.12}$$

with M a proportionality constant. Using (2.2), (2.11) and (2.12), the admittance data from a HO device is fitted, as shown in figure 2.1. At low and high frequencies the theory fits well with the data, however for $\omega \approx \tau^{-1}$ and low bias the theory overestimates the inductive

[1] Note the square of $\tilde{\mu}$ in the denominator, which is not present in the original paper [MBP99].

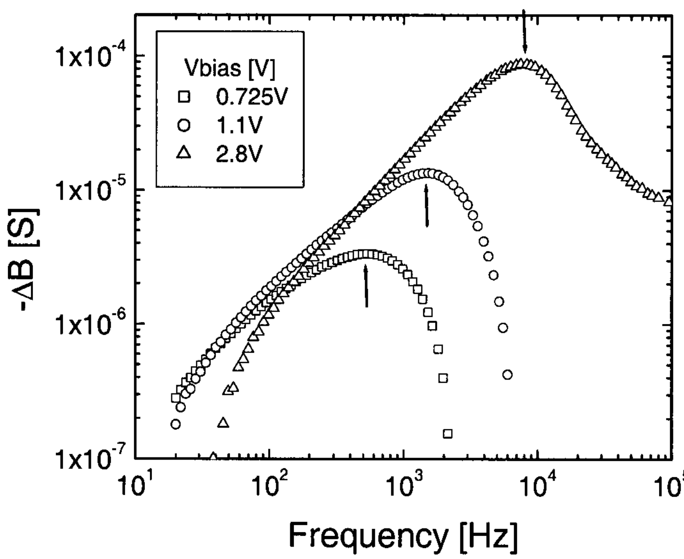

Figure 2.2: The negative differential susceptance of a hole-only device. The arrows indicate the resonance frequency ω_{res}.

effect. Note that for higher bias the discrepancy becomes less. The cause of the discrepancy is that dispersive transport not only gives a frequency dependent mobility, but also results in a broad distribution of transit times, τ, of individual carriers that will "smear out" the inductive contribution. Such a transit time distribution is described in ref [MBP99], but is not yet incorporated in the present work.
From the fits of data in figure 2.1 we obtain the following values for the parameters in (2.2): $\alpha = 0.52$ and $M = 0.067$. The negative contributions to C are clearly visualized when the negative differential susceptance

$$-\Delta B = -\omega \left(C - C_{bi}\right) \tag{2.13}$$

is plotted, as shown in figure 2.2. Here we use the capacitance for $V_{bias} = V_{built-in}$ (C_{bi}) as reference. This in contrast to Martens et al. [MHB00] who use the zero-volt capacitance (C_0) as a reference. The reason to use C_{bi} instead of C_0 is that for $V_{bias} = V_{built-in}$ the device is in the flat-band condition. From this point on to higher bias, charge carrier transport takes place. It is this transport that induces the negative contribution to the capacitance. This choice of reference becomes even more important when studying dye-doped double-carrier devices. It will be shown that $V_{built-in}$ depends on the concentration of dye-doping, so if we want to make a comparison between devices with different dye concentrations, the internal fields ($V_{bias} - V_{built-in}$) must be the same.

In figure 2.2 a single relaxation peak visualizes the inductive contribution of the holes. From the fits in figure 2.1 we obtain the relaxation time τ and from the peak positions in figure 2.2 we obtain the resonance frequency $f_{res} = \omega_{res}/(2\pi) = 1/(2\pi\tau_{res})$. In table 2.1 a few of these values are summarized. It shows that the maximum of the relaxation peak

$V_{bias}[V]$	$\tau_{res}[s]$	$\tau[s]$	$\frac{\tau_{res}}{\tau}$
0.725	$2.97 * 10^{-4}$	$9.5 * 10^{-4}$	0.31
1.1	$1.04 * 10^{-4}$	$4.2 * 10^{-4}$	0.25
2.8	$2.03 * 10^{-5}$	$7.6 * 10^{-5}$	0.27

Table 2.1: Relaxation times.

$\omega_{res}^{-1} = \tau_{res} \approx 0.28 \times \tau$, which is in close agreement with previous studies where a factor of 0.29 was found [MBP99]. The factor 0.28 is a consequence of the non-homogeneous field distribution in the device; for a homogeneous distribution the relaxation peak would be located at $\tau_{res} = \tau$. The mobility can now be deduced from the data by determining the peak position of the relaxation peak:

$$\mu = \frac{L^2}{\tau_{res} V} \approx 1.8 \frac{L^2 f_{res}}{V}, \tag{2.14}$$

with f_r the resonance frequency.

2.2 Conclusions

Finally we can conclude that the mobility of holes in a HO device can be obtained not only by fitting (2.11) to the complex part of the admittance data, but also by determining the peak positions of the relaxation peaks in the $-\Delta B$ plots, which is a very quick and elegant way of determining the charge carrier mobility. The reference capacitance used for $-\Delta B$ is obtained at $V_{bias} = V_{built-in}$.

CHAPTER 3

Charge Carrier Dynamics in Dye-Doped PLEDs - Experiment

In this chapter the results of three different measurements performed on polymer light-emitting diodes are discussed:

- The compensation voltage,
- capacitance vs bias measurements,
- and hole mobility measurements.

They all have one thing in common and that is that they can be used to determine the influence of dye-doping on the charge-carriers. Because we have the disposal of both double-carrier and hole-only devices we can do the same experiments on both devices and relate the results to the presence of a single carrier (holes) or to the presence of holes as well as electrons. On top of that we can also vary the degree of molecular doping in both kind of devices, which enables us to evaluate the concentration dependence of dye-carrier interactions.

3.1 Sample Preparation

For our experiments we used two types of diode structures, BaAl-PPV-PEDOT-ITO for the double-carrier devices and Au-PPV-PEDOT-ITO for the hole-only devices. The samples were prepared in a glove box under N2 atmosphere. A polymer/toluene solution containing 4.5 mg/ml polymer is stirred at room temperature over night and heated at 70°C for 1 hour before the dye is added from a stock solution in toluene (4 mg/ml). The polymer + dye/toluene solution is stirred at room temperature for 1 hour and filtered over a 5 mm PTFE filter (Millex, Millipore). The glass substrates, patterned with a 120 nm transparent ITO layer (20 $\Omega/\Box$), were treated for 10 min with UV/O3 (UVP PR-100) prior to spin coating. Remaining dust particles are blown away with ionized nitrogen before 150±5 nm of a conductive polymer (poly(3,4 ethylenedioxythiophene:polystyrene sulphonic acid, PEDOT:PSS, from Bayer AG) and 705 nm of the emissive layer are spin coated on the substrates. The layer thicknesses are measured using a Dektak ST surface profile measuring system. In these devices, the

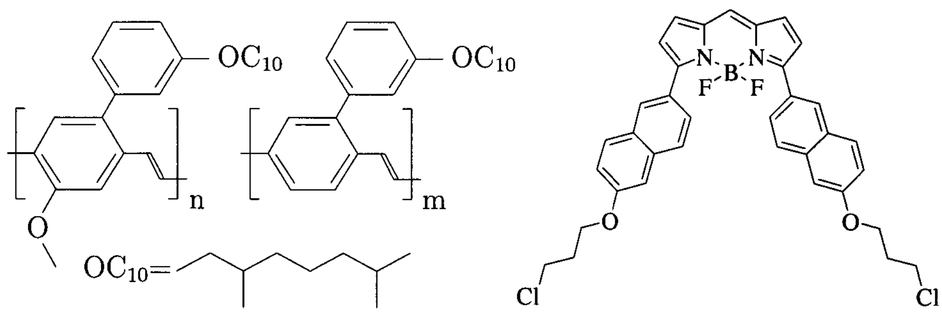

Figure 3.1: The chemical structure of the yellow-PPV, the polymer used in the PLEDs (left). The chemical structure of the red dye (right).

ITO/PEDOT:PSS stack serves as anode. A Ba/Al cathode for double carrier devices and an Au cathode for hole only devices is applied by vacuum evaporation using a self-built evaporation chamber. All devices are sealed to exclude oxygen and water during the measurements. The yellow emitting PPV-based polymer was prepared via the Gilch polymerization route and has been described in detail elsewhere [Bec00]. The chemical structure of the polymer and the dye are shown in figure 3.1.

3.2 Admittance Spectroscopy

Admittance (or impedance) spectroscopy is a means to study charge transport dynamics in solid state devices. The general approach in admittance spectroscopy is to apply an electrical stimulus (voltage or current) and monitor the response. Mostly the admittance is determined in the frequency domain, by applying an ac voltage of frequency ω and measuring the amplitude and phase shift of the resulting current. The complex admittance is defined as in equation (2.1). The real part of Y represents the in-phase Ohmic current, while the imaginary part reflects the out-of-phase component of the response.

In this study, admittance measurements in the range 20Hz - 1MHz were performed using an Agilent 4284a RCL impedance analyzer. The analyzer can superimpose a bias voltage varying from -30V to +30V on top of the ac voltage. The capacitance-voltage characteristics were measured with at constant frequency of 20Hz. The ac voltage on top of the bias was 50mV. The capacitance was checked to be independent of the ac voltage in the range of 10mV to 100mV.

3.3 The Compensation Voltage as a Function of Dye Concentration in PLEDs

Due to the difference in work functions of the cathode and anode an internal electrical field will be present in the polymer layer of a (asymmetrical) PLED upon device fabrication. This electric field or built-in potential (V_{bi}) prevents the injection of charge carriers of the proper sign into the polymer. The compensation voltage, V_0, of a PLED is defined as the voltage

where no current flows through the device. At V_0 the external field and internal field cancel each other and flat band condition is achieved. Decreasing the voltage below V_0 reverses the field in the device. The LED is now operating under backward bias. Increasing the voltage beyond V_0 puts the LED in forward bias and charge injection can take place. Excitons that are formed under these conditions in the polymer layer, split up and generate a drift current, which is generally referred to as photo current (I_{photo}). The total current under illumination (I_{light}) then comprises of this photocurrent, a diffusion current and a leakage current (at $V_{bias} \neq 0$). Under exclusion of light only the diffusion current and leakage current remain, the total is called the dark current (I_{dark}). By sweeping the bias from below V_0 to above V_0 under both illumination (I_{light}) and dark (I_{dark}) conditions and subtracting the two, $I_{photo}(V_{bias})$ is obtained. The sign of this photo current gives information about the field in the device. The photo current changes sign at $V_{bias} = V_0$.
According to Malliaras *et al.* [MSBS98] the compensation voltage at which the net photocurrent is zero is

$$V_0 = V_{bi} - \frac{k_B T}{e} \ln \frac{\mu_e g_{e,c} + \mu_h g_{h,a}}{\mu_e g_{e,a} + \mu_h g_{h,c}} \tag{3.1}$$

where $g_{e,c}$ ($g_{e,a}$) is the density of photogenerated electrons at the cathode (anode) per unit of light intensity, $g_{h,c}$ and $g_{h,a}$ are the same but now for the holes. The assumption is that the excitons in the semiconducting polymer are tightly bound and dissociate via transfer of charge to the metal electrode, leaving the other charge free inside the organic layer. Therefore bulk photogeneration of charge is neglected.

The compensation voltage is a function of a multitude of factors such as the built-in potential (Vbi) due to the work function difference of the contacting electrodes, the competition between the diffusion and the drift of the photo-generated carriers [MSBS98] and the barrier height at the electrode-semiconducting polymer interface. This interface can be modified by interface defects and structure related interface dipoles. Blending a dye into the semiconducting polymer (referred to as molecular doping in the literature) changes the energetical landscape in the bulk as well as at the interfaces. In general these dyes are chosen to work as emissive center and/or to facilitate charge transport of one charge carrier. Either way they present a potential trap for charges since in order to fulfill their function they have to interact with the charges or excitons and can furthermore act as acceptors at the electrode interface even below the bias at which the flat band condition is achieved. Adding dopants modifies the carrier transport and the injecting interface and should therefore influence the compensation voltage in one way or another. Thus by studying V_0 as a function of dopant concentration one should be able to gain information about the interface barrier and charge transport behavior.
Let us assume that the molecular dopant added to the semiconducting polymer has an energy level that can act as a trap for electrons, that is the dopant LUMO lies below the polymer LUMO and that the HOMO levels of polymer and dopant are aligned. The dopant is added in such low concentrations to the polymer that it is homogeneously dispersed and the dopant percolation limit is not reached. If the dopant can act as electron acceptor and the chemical potential of the contacting cathode allows for it, electrons can be transferred (tunnel) from the metal to the acceptor dopant and a dipole layer is formed, which modifies the interface as sketched in figures 3.2 and 3.3. Since there is no percolation of the dopant, the transport is limited to the bulk interface layer. In literature this modification is also refered to as vacuum level shift [SSKP02].

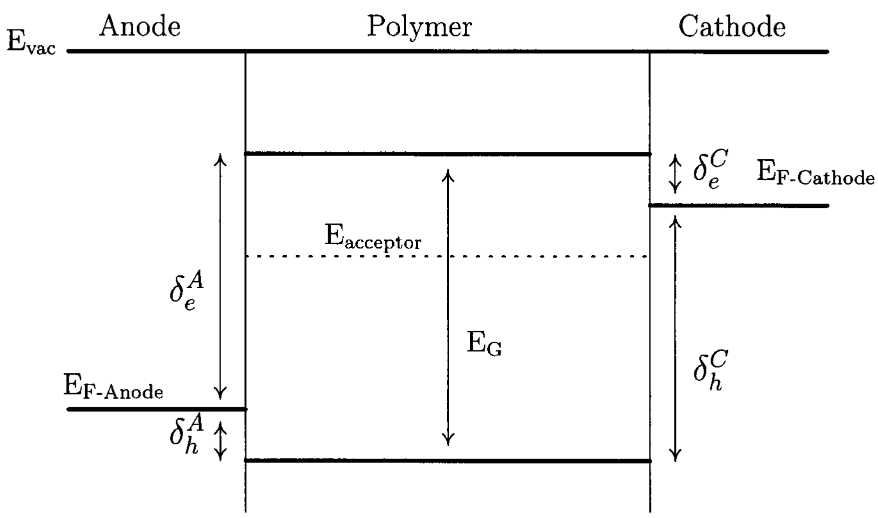

Figure 3.2: Ideal band structure of a PLED at the built-in potential V_{bi}. The polymer is described as dielectric without any charge exchange with the electrodes. E_G is the HOMO-LUMO distance of the polymer, $E_{acceptor}$ is the LUMO level of the molecular dopant. $E_{F-Anode}$ and $E_{F-Cathode}$ are the Fermi levels of the anode and the cathode respectively, δ_e and δ_h are the electron and hole barriers respectively for injection into the polymer LUMO or HOMO levels of the semiconducting polymer. E_{vac} is the vacuum level.

V_{bi} can be described as an function of the electron (hole) barrier at the anode and the electron (hole) barrier at the cathode. For the definition of the symbols see figure 3.2.

$$V_{bi} = \delta_e^a - \delta_e^c = \delta_h^c - \delta_h^a \tag{3.2}$$

Any change in barrier height will result in a modification of the built-in potential and thus of the compensation voltage, see figure 3.3. The modified barrier is

$$\delta_e^{c*} = \delta_e^c + \Delta\Phi \tag{3.3}$$

The potential drop due to charge accepted by the dopant in the polymer at the polymer-cathode interface can be described analogously to the potential drop of a parallel-plate capacitor:

$$\Delta\Phi = \frac{eN^*d}{\epsilon_0\epsilon}, \tag{3.4}$$

where ϵ, N^* and d are the dielectric constant, the number of dopant molecules that have accepted an electron per unit area and the average distance of the accepted charges to the cathode, respectively. For the compensation voltage we finally write

$$V_0 = V_{bi} - \Delta V_{photo} - \Delta\Phi \tag{3.5}$$

with ΔV_{photo} the correction term of V_{bi} in equation (3.1).

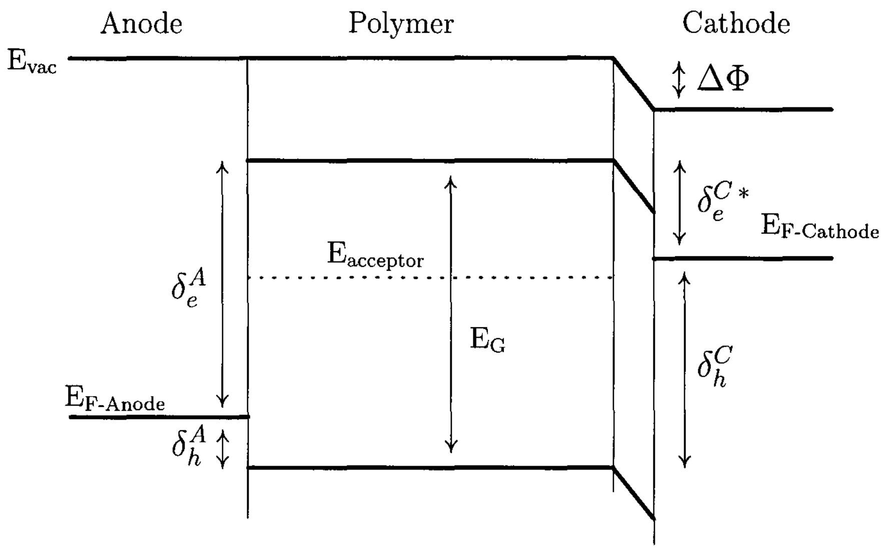

Figure 3.3: Modification of the cathode interface by a dipole layer at the cathode. The molecular dopant acts as electron acceptor if the electrochemical potential of the cathode allows for it.

3.3.1 Resistance measurements

The built-in potential can also be determined by looking at the resistance of the PLED as a function of the applied bias. The resistance is measured by impedance spectroscopy at 20Hz. For $V_{bias} < V_{bi}$ the resistance is constant, at a certain point the resistance drops dramatically. From this point on charge transport through the device is possible which indicates a flat-band condition. The bias at this point is said to be V_0. By plotting dR_p/dV the sudden drop in resistance is revealed by the peak position, see figure 3.4.

3.3.2 Results

Figure 3.5 shows the results of the compensation voltage measurements for different dye mass ratios, performed on double carrier devices. According to the photovoltaic measurements V_0 decreases for increasing dye mass ratio. Looking at equation (3.5) this can be due to a change in the the density of photogenerated charge carriers and/or change in the charge mobility or due to the formation of a dipole layer. However, for hole-only devices there is no effect of the dye on V_0 (cf. figure 3.6), despite of the fact that it was measured under identical conditions. The only difference between the HO and DC devices is the work function of the cathode. The Fermi level of BaAl (DC) is higher than the LUMO of the dye and therefore acts as an electron donor. The Fermi level of Au lies beneath the LUMO of the dye and acts as an electron acceptor. So the forming of a dipole layer in the DC devices is the only plausible explanation of the potential drop. The general trend of decreasing V_0 in DC devices is reproduced by the resistance measurements, although for low dye concentrations (<1%) V_{bi} is underestimated and for higher concentrations (>1%) V_{bi} is overestimated.

From equation (3.4) and the photoluminescence data of figure 3.5 we can make an estimate

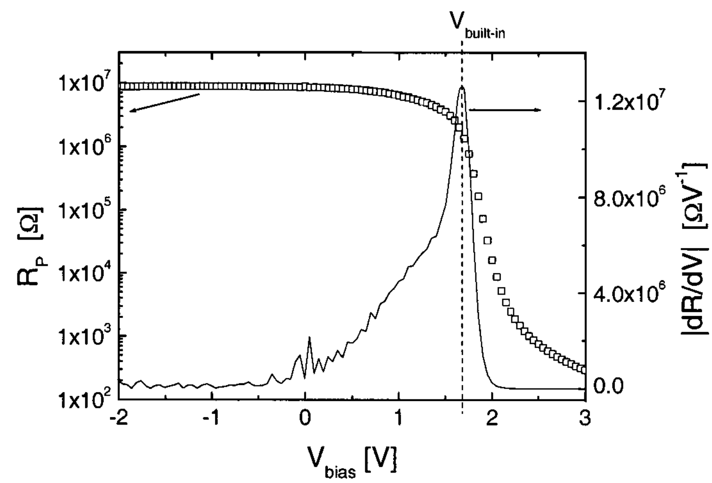

Figure 3.4: Parallel resistance (R_p) and dR_p/dV as a function of V_{bias}, measured by impedance spectroscopy at 20Hz.

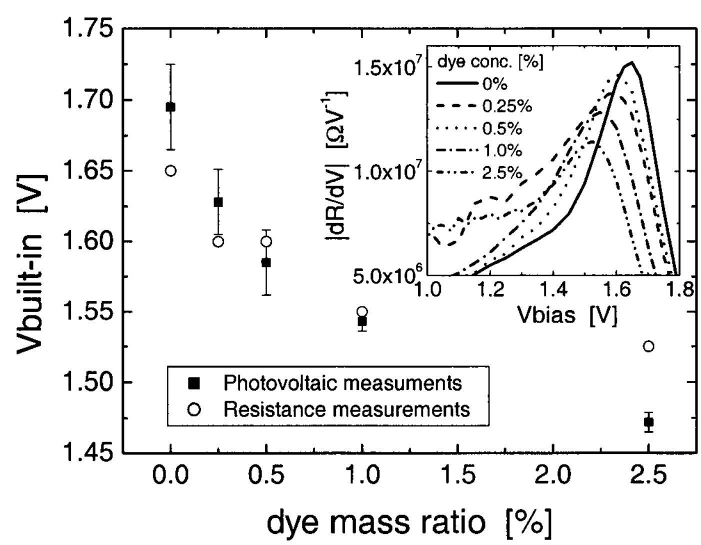

Figure 3.5: Photovoltaic measurements of the compensation voltage as function of the dye mass ratio, performed on double-carrier devices. The inset shows dR_p/dV for various dye mass ratios, the peak positions determine V_0.

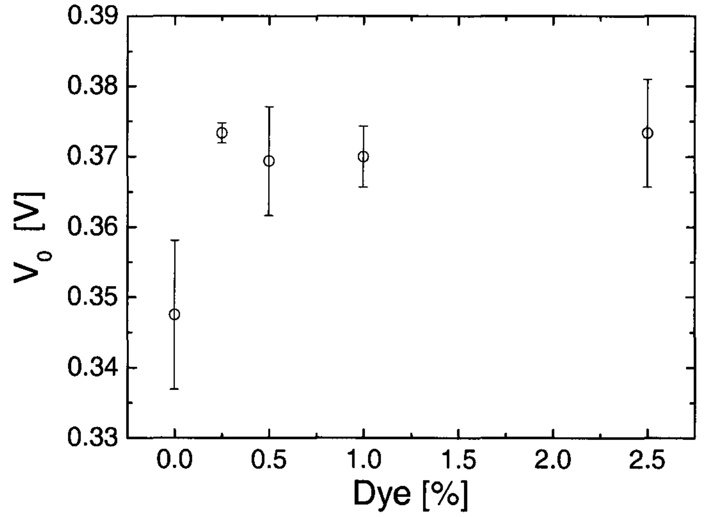

Figure 3.6: Photovoltaic measurements of the compensation voltage, V_0, as function of the dye mass ratio, performed on hole-only devices.

$\Delta\Phi\,[V]$	$c\,[\%]$	$N\,[m^{-2}]$	$N^*\,[m^{-2}]$	N^*/N
0.07	0.25	$1.5 * 10^{17}$	$2.7 * 10^{16}$	0.18
0.11	0.5	$3.0 * 10^{17}$	$4.3 * 10^{16}$	0.14
0.16	1.0	$6.0 * 10^{17}$	$6.2 * 10^{16}$	0.10
0.23	2.5	$1.5 * 10^{18}$	$8.9 * 10^{16}$	0.06

Table 3.1: Estimate of the fraction of dye molecules that accept an electron at the polymer-cathode interface. With c the mass percentage of dye molecules, N the number of dye molecules per unit of area and N^* the number of dye molecules per unit of area that have accepted an electron. Other parameters are $d = 5\text{Å}$, $\epsilon = 3.5$, the polymer density $\rho_{pol} = 1.19\text{g/cm}^3$ and the dye molar mass $\rho_{dye} = 833\text{g/mol}$.

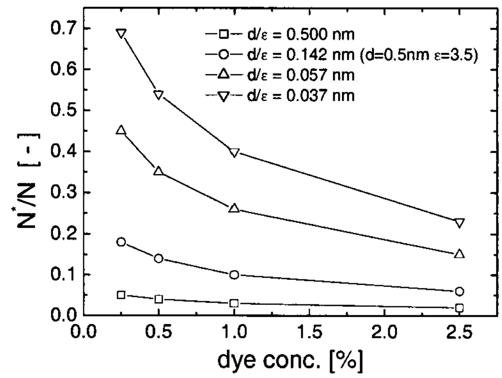

Figure 3.7: Influence of d/ϵ on the fraction of dye molecules at the cathode surface that accept an electron.

of the fraction of dye molecules that accept an electron at the polymer-cathode interface, these are tabulated in table 3.1. We see that N^*/N decreases with the dye concentration. Apparently there will be a saturation point at which adding more dye will have little or no effect on V_0. A possible explanation is that the driving force for the tunnelling of the electrons to the dye is the energy difference $\Delta = E_{F-Cathode} - E_{acceptor}$. Due to the vacuum level shift Δ becomes less. For even higher dopant concentrations the percolation limit will be reached and Δ will be zero, this is the so called Fermi level pinning. The exact values of the parameters ϵ and d are not know to us. However in figure 3.7 the influence of d/ϵ on N^*/N is plotted.

The most important conclusion we can make is that the influence of the dye on the compensation voltage is no bulk effect but due to modification of the bulk-cathode interface.

3.4 Capacitance Measurements

By studying the capacitance of a PLED as a function of bias we can draw general conclusions of the influence of dye-doping on the charge carriers.
The capacitance of both hole-only (HO) and double-carrier (DC) devices was measured as a function of applied bias using impedance spectroscopy. These measurement will hereafter be referred to as $C(V)$ measurements.
We will first discuss the results of measurements on a HO device. Looking at figure 3.8 we see at low bias (<0V) that the capacitance is constant and equals the geometrical capacitance, $C_0 = \varepsilon A/L$. Above 0V the capacitance increases to a maximum at $V_{bias} = 0.4V$. Increasing the bias causes the capacitance to decrease until it reaches a minimum ($C_{min} > C_0$). Finally for even higher bias the capacitance increases constantly.
For the DC device we see almost the same characteristics. At low bias the capacitance also equals the same geometrical value, but the maximum is now shifted 1.53V towards higher bias. After the maximum the capacitance drops to a minimum (of negative capacitance) after which the capacitance increases again. The inset of figure 3.8 shows the resemblance of the $C(V)$ curves when the HO curve is shifted to overlap the maxima. The fact that the maxima of the curves overlap so well can be an indication that there is no effect of the cathode on

this and that the maximum is solely due to interaction of the polymer and anode.
Upon doping of the DC device we see that the minimum of the capacitance shifts towards higher values (cf. figure 3.9). For high dye concentrations the characteristics of the dye-doped DC devices even starts to resemble those of a HO device (the solid line in). This can be explained in terms of electron trapping. More dye in the bulk means that more electrons get trapped and that the only mobile charge carriers in the sample are the holes. That the holes have no interaction with the dye follows from figure 3.10.
Summarizing we can conclude that:

- The main difference of the C(V) characteristics between HO and DC devices (apart from the overall shift to higher bias for the DC devices) is the (large) negative minimum of the DC devices.
- The existence of this negative minimum can be attributed to the electrons present in the DC devices.
- The upward shift of the minimum upon doping is due to electron trapping on the dye. Such a shift is not observed for the HO devices.
- The occurrence of a maximum in the curves is due to interaction of the polymer with the anode, changing the (work function of the) cathode has no influence other than the shift towards higher bias for the DC device.

The shift of the maximum towards higher bias of the DC compared to the HO could be a consequence of the different work functions of the cathodes. However, there is no shift of the maximum of the DC devices upon molecular doping as observed in the measurements of the compensation voltage (cf. section 3.3).
For high bias there is a constant increase of the capacitance for both HO and DC devices. The internal field of the device is such that the space charge limited current (SCLC) regime is entered. In this regime charges that are injected into the bulk will accumulate there and not immediately traverse the bulk. For higher bias more charge can be accumulated in the bulk: $C = \mathrm{d}Q/\mathrm{d}V$.

3.4.1 Theoretical Model

In the following we give a qualitative model for the $C(V)$-characteristics of HO devices. In figure 3.11 the situation is sketched after the device has been made. All the Fermi levels are aligned and there is an internal field due to the work function differences of the electrodes. The cathode interface is neglected in the model due to the arguments summarized above and is only used to define a voltage drop across the device. To align the Fermi levels, holes are accumulated in the device and band bending at the anode interface occurs. There is now a competition between diffusion and drift current and eventually a steady state is reached. There will be a specific region at the interface with accumulated charge carriers and a specific thickness w. Since the interface is charged with holes, it can be thought of as an extension of the anode. This interface directly modifies the capacitance of the device, the geometrical capacitance $C_0 = \varepsilon A/(L - w)$ increases due to the increase of w.
In figure 3.12 the situation is shown when the voltage is increased (forward bias). The field in the bulk will diminish as well as the drift current. The result of this is an increase of the width w of the region with accumulated charges and therefore an increase of the capacitance.

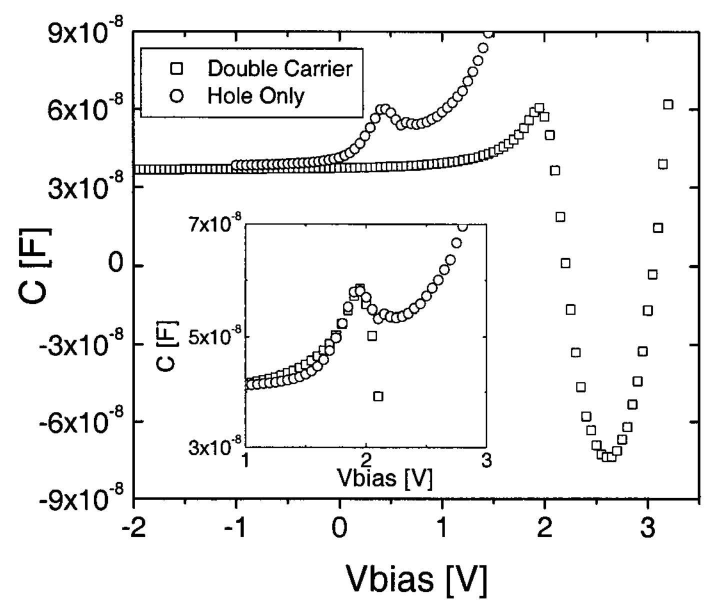

Figure 3.8: Capacitance of a hole-only and double-carrier device as a function of the applied bias. The inset shows the same data with the hole-only curve shifted 1.53V to match the double-carrier curve.

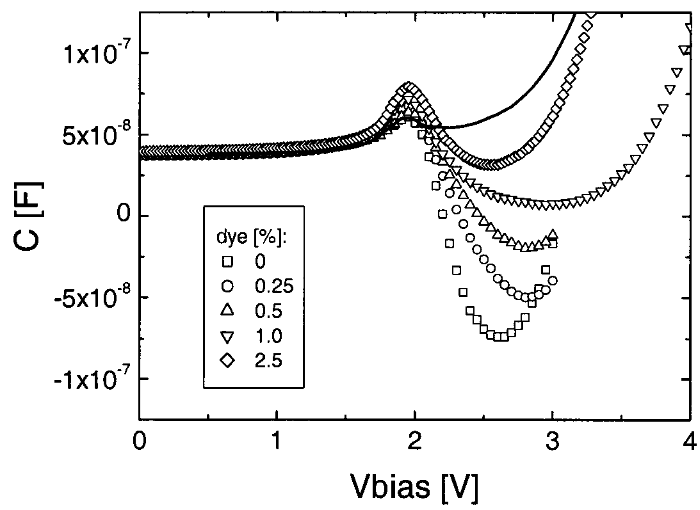

Figure 3.9: Influence of dye-doping on the capacitance of double-carrier devices. For comparison a (shifted) HO curve was added (solid line). For high dye concentration the $C(V)$ characteristics of the double-carrier device resemble those of the hole-only device.

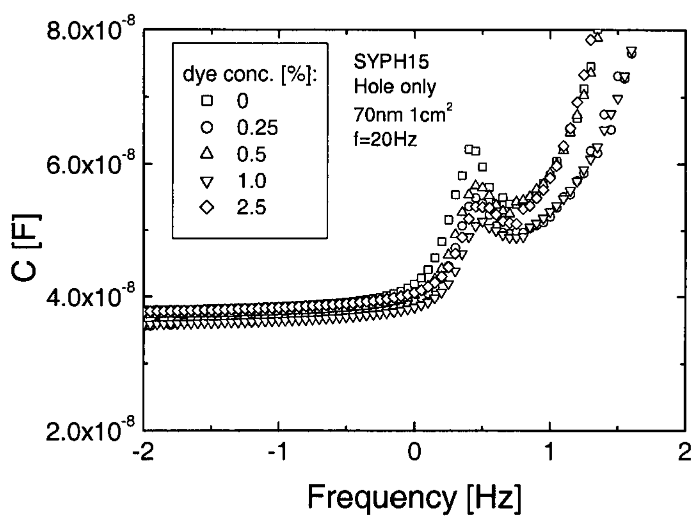

Figure 3.10: Influence of dye-doping on the capacitance of hole-only devices. No significant change upon doping can be observed.

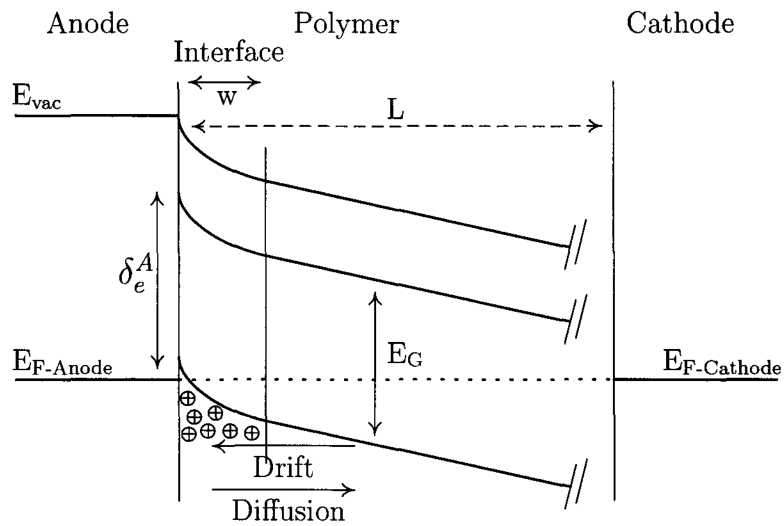

Figure 3.11: Band structure of a PLED with no applied bias. Holes are transported from the anode to the interface region and form a accumulation of charge causing band bending in the interface region. In the stationary situation, as sketched, the diffusion and drift current cancel each other.

Near the flat band condition in the bulk the maximum width w is expected and therefore the maximum capacitance. It is clearly seen that the effect scales with the internal field, not the external. Figure 3.13 shows what happens if the field is increased beyond the onset. The drift and diffusion current are now in the same direction, though there is still a drift in the interface region in the opposite direction. Before the onset of SCLC there will be a field region where the interface region is emptied. The charges in this region now drift to the cathode and the interface region diminishes, causing the capacitance to decrease again. Exactly this can be seen in the $C(V)$ measurements. By further increasing the field the space charge limited region is entered and the capacitance increases again.
Some preliminary results show only an increase of the capacitance of approximately 10% instead of the 50% found experimentally.

Another model proposed by Hulea *et al.* treats the contact-polymer interface as a Schottky barrier. The device is modelled as two parallel resistance and capacitance circuits in series, mimicking a depleted junction and the undepleted bulk. The assumption of the Schottky theory implies that there are free charge carriers present in the bulk. It is still under discussion whether this is the case in the devices we have studied.

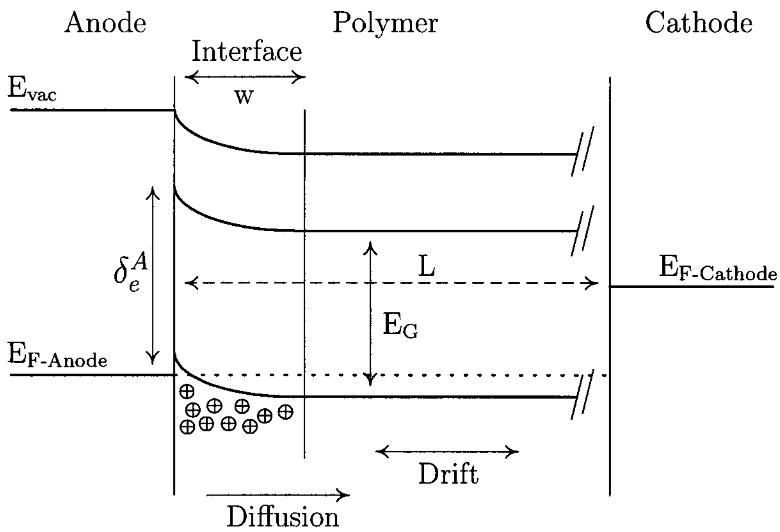

Figure 3.12: As figure 3.11. The bias is such that flat band condition is achieved. The width of the interface layer has increased.

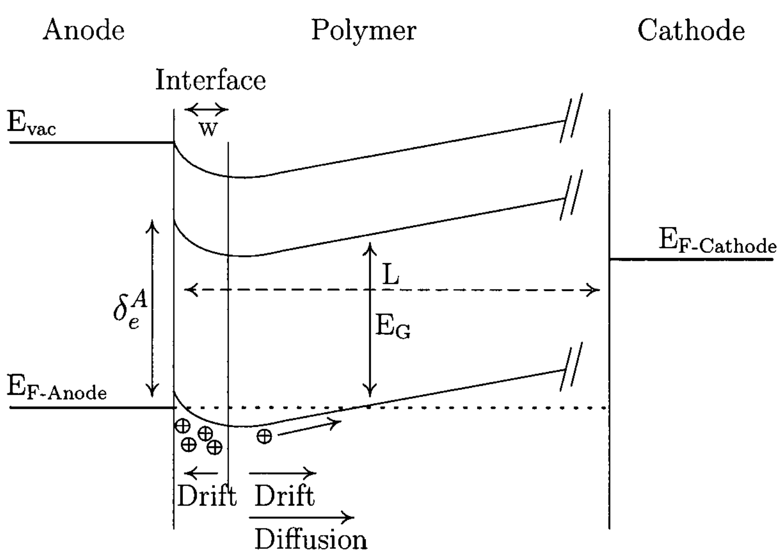

Figure 3.13: By further increasing field the device in in forward bias and the interface layer diminishes.

	γ $[(m/V)^{1/2}]$	μ_0 $[(m^2/Vs]$
Hole-Only	$3.5 * 10^{-11}$	$2.0 * 10^{-4}$
Double-Carrier	$4.5 * 10^{-13}$	$6.8 * 10^{-4}$

Table 3.2: Field dependence and zero-field mobility of the hole mobility in a HO and DC device.

3.5 Charge Carrier Mobility from Admittance Spectroscopy

In section 2.1 we have shown that the hole mobility of holes in a hole-only device can be obtained using admittance spectroscopy. The same technique is used for double-carrier devices (PLEDs). It has been shown that, using this technique, both electron and hole mobilities can be measured simultaneously [MHB00]. The results of hole mobility measurements for hole-only devices and double-carrier devices will be compared.
Many studies of hole transport in conjugated polymers show that the hole mobility can be described by the empirical relation

$$\mu = \mu_0 \exp\left(\gamma\sqrt{E}\right) \tag{3.6}$$

with E the electric field, μ_o the zero-field mobility and γ a field activation factor.

3.5.1 Frequency Dependent Response of PLEDs

In figure 3.14 the capacitance as a function of frequency of a PLED is plotted. For $V_{bias} = 0$V the capacitance is constant. For $V_{bias} > V_{built-in}$ again an inductive effect can be seen for the lower frequencies. Taking a closer look at this effect by plotting $-\Delta B = -\omega\left(C - C_{bi}\right)$ reveals two relaxation peaks, one of the electrons one of the holes. Unfortunately the width of the electron peak is too large to be able to accurately determine the peak position, therefore it was not possible to determine the electron mobility.
The mobility of the holes for increasing internal field E are determined by the peak positions of the 'hole peaks' and eq. (2.14) and plotted in figure 3.15. For comparison we have added the hole mobility obtained from a hole-only device. Their values of γ and μ_0 are presented in table 3.2.

Compared to the HO device the field dependence of hole mobility in the DC device is much different. The zero-field mobility is lower and the field dependence is larger. Such a large discrepancy between the hole mobility in HO and DC devices has not been observed before. Possible explanations are:

- Due to the presence of electrons in the bulk the field distribution in differs from that of a HO device.
- Due to the recombination of charge carriers the dispersion of the hole mobilities is changed.
- An artefact of the method of determining $-\Delta B$. Here we use C at $V_{bias} = V_{bi}$ as a reference instead of C at $V_{bias} = 0$V as was done in previous studies [MPB+01]

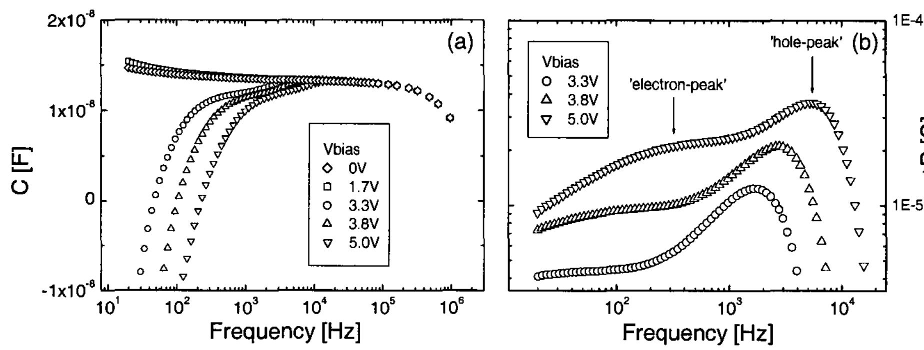

Figure 3.14: (a) Frequency dependence of the capacitance of a PLED as function of bias voltage, $V_{built-in} = 1.7\text{V}$. (b) Negative differential susceptance, $-\Delta B$, as a function of frequency, two relaxation peaks can be distinguished for electron and hole transport.

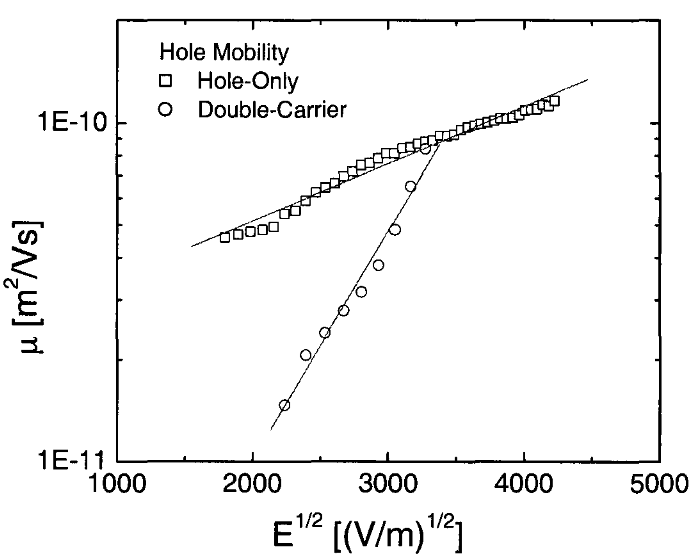

Figure 3.15: Field dependence of hole mobility in both hole-only and double-carrier devices. The solid lines are linear fits to the data.

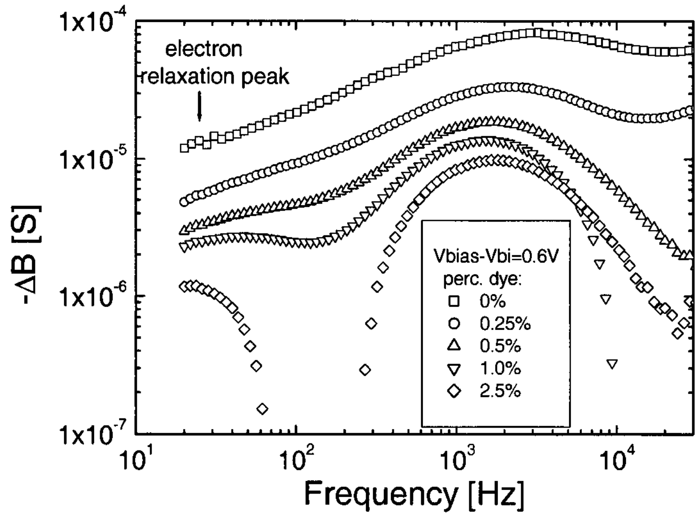

Figure 3.16: Negative differential susceptance of dye-doped PLEDs. We see that the electron peak becomes more pronounced for higher dye concentrations, indicating that the dispersion of the transit times of the electrons becomes less.

3.5.2 The Influence of Dye-Doping on Charge Carrier Mobility

In figure 3.16 the negative differential susceptance of dye-doped PLEDs is plotted. The electron relaxation peak shows some interesting features when plotted as function of dye concentration. The relaxation peak of the electrons narrows as the concentration increases indicating that the dispersion of transit times of the electrons becomes less. Unfortunately we cannot measure below 20Hz but from the data it can be clear that there is a small separate electron relaxation peak around 22Hz. This narrowing can be explained in terms of trapping of the electrons by the dye molecules. Only the electrons with mobility around μ_{dc} can traverse the device, the faster and slower electrons are trapped by the dye molecules. The shape of hole peak is not affected as much as the electrons, only the peak position shifts to lower frequencies for higher dye concentrations. The increase of $-\Delta B$ for 0% and 0.25% for $f > 2 * 10^4$Hz is not due to relaxation of charge carriers, but can be explained by the fact that by calculating $-\Delta B$ (2.13) the difference between two capacitance curves is multiplied by a large number, ω.

The field dependent hole mobility in a HO device is plotted as a function of dye concentration in figure 3.17. There is no noticeable effect of the concentration on the mobility. However, looking at the same quantity in a double carrier device, figure 3.18, we see a distinct effect of dye concentration on the mobility. For increasing dye concentration the zero-field mobility, μ_0, increases and the field dependence, γ, decreases. The values of γ and μ_0 of both hole-only and double-carrier devices are summarized in table 3.3. Again we see that for increasing dye concentration the characteristics of a double carrier device tends towards those

	Hole-Only		Double-Carrier	
conc. dye [%]	γ $[(m/V)^{1/2}]$	μ_0 $[(m^2/Vs]$	γ $[(m/V)^{1/2}]$	μ_0 $[(m^2/Vs]$
0.0	$1.7 * 10^{-4}$	$2.3 * 10^{-11}$	$6.8 * 10^{-4}$	$4.5 * 10^{-13}$
0.25	$1.7 * 10^{-4}$	$2.1 * 10^{-11}$	$5.1 * 10^{-4}$	$1.3 * 10^{-12}$
0.5	$1.6 * 10^{-4}$	$2.4 * 10^{-11}$	$4.0 * 10^{-4}$	$2.1 * 10^{-12}$
1.0	$1.6 * 10^{-4}$	$1.9 * 10^{-11}$	$4.0 * 10^{-4}$	$1.6 * 10^{-12}$
2.5	$1.5 * 10^{-4}$	$2.6 * 10^{-11}$	$3.3 * 10^{-4}$	$3.0 * 10^{-12}$

Table 3.3: Field dependence, γ, and zero-field mobility, μ_0, of holes in hole-only and double-carrier devices as a function of dye concentration.

of a hole-only device [1].

[1]During the writing of this report there was still an ongoing discussion about the right value of the built-in potential of the dye-doped PLEDs, therefore an additional graphs concerning this discussion are presented in appendix A.

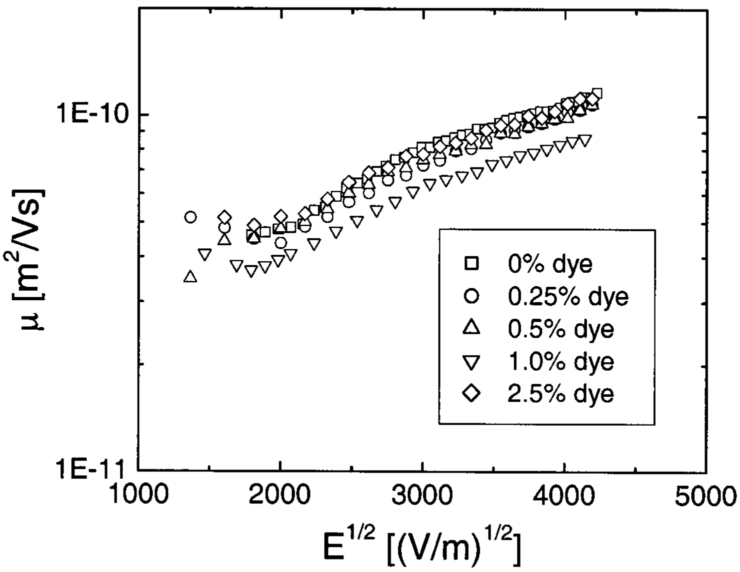

Figure 3.17: Mobility of holes in a hole-only device as a function of dye concentration.

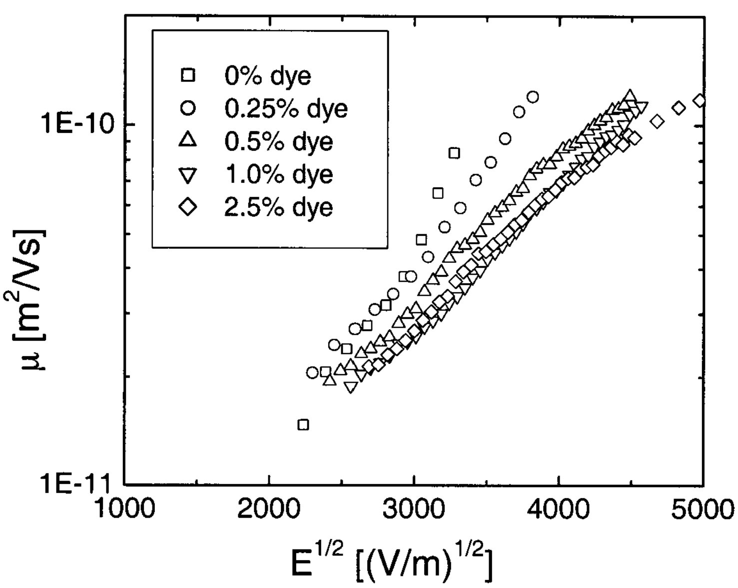

Figure 3.18: Mobility of holes in a double-carrier device as a function of dye concentration.

3.6 Conclusions on the Charge-Carrier Dynamics

The following conclusions can be made from the results described in this chapter:

- Upon molecular doping the change in compensation voltage (V_0) in double-carrier devices is measured by two independent methods, i.e. photovoltaic measurements and resistance measurements.

- The change in compensation voltage (V_0) in double-carrier devices upon molecular doping is due to modification of the polymer-cathode interface. The work function of the cathode plays a crucial role, only devices with low work function cathodes (electron injectors) show a change in V_0.

- By adding molecular dopants the $C(V)$ characteristics of a double-carrier device tend to those of a hole-only device. This is an indication that the dye acts as a trap for electrons.

- Hole mobilities derived from the negative differential ($-\Delta B$) curves from hole-only and double-carrier devices have different field dependencies. The values of μ_0 and γ of the hole-only device are in good agreement with the values generally found in the literature. This can be explained by the fact that in the double-carrier device electrons are present in the bulk, which changes the field distribution. Also recombination could play a role in the change of the mobility.
  Another possibility is that it is an artefact of the method of determining $-\Delta B$, i.e. $C(V_{built-in})$ is not a good reference.

- The negative differential susceptance of a double-carrier device shows narrowing of the electron peak upon doping, which is also an indication of electron trapping. No significant effect is seen on the width of the hole peak.

- The hole mobility of holes in hole-only devices is not affected by molecular doping.

- The hole mobility of holes in double-carrier devices is affected by molecular doping. The values of μ_0 and γ tend to those of hole-only devices for high doping concentrations.

CHAPTER 4

Exciton Transport in Polymer and Polymer-Dye Systems

In this chapter we study the diffusion of excitons in a constant DOS and a Gaussian DOS. For both an expression for the diffusivity for various temperature regimes will be derived.

4.1 Exciton Transport in Polymers

In most of the conjugated polymeric systems chemical and mechanical defects on the polymer chain limit the delocalization of the excitons along the chain. The position of these defects is more or less random, which results in a rather broad distribution of the effective conjugation length of the chain segments separated by the defects. As the energy of excitons depends strongly on the effective conjugation length of the chain segment on which they are residing, the distribution of conjugation lengths translates into a strongly inhomogeneous broadened density of states (DOS) for these particles. So, due to the disorder, the excitons are strongly localized and their transport can generally be modelled as incoherent hopping between localized states.

Absorption (and fluorescence) bands of disordered organic solids are assumed to be of Gaussian shape with a standard deviation of typically σ=70meV [MHOB01]. Therefore the inhomogeneously broadened DOS of the excitons are modelled by a Gaussian shape with the same Gaussian width σ

$$g(\varepsilon) = \frac{1}{\sigma\sqrt{2\pi}} exp\left(-\frac{\varepsilon^2}{2\sigma^2}\right). \tag{4.1}$$

The hopping rate among sites i and j is assumed to be of the Förster type, the product of the inverse lifetime of the excitons k_0, spatial dependence due to the dipole-dipole interaction and a Boltzmann factor for jumps upward in energy [Dex53]

$$v_{ij} = \begin{cases} k_0\left(\frac{R_0}{R}\right)^6 exp\left(-\frac{\epsilon_j-\epsilon_i}{k_B T}\right) & \text{if } \epsilon_j > \epsilon_i, \\ k_0\left(\frac{R_0}{R}\right)^6 & \text{if } \epsilon_j < \epsilon_i. \end{cases} \tag{4.2}$$

Equation (4.2) implies that the coupling to the heat bath is sufficiently strong. Hops down in energy are not impeded by an energy matching condition for dissipation of the electronic energy difference.

4.2 Exciton Diffusion in a Constant DOS - Mott Hopping

In this section the diffusion in a constant DOS is studied. Later on in section 4.3 this will be expanded to a Gaussian DOS.

According to (4.2) the probability of hopping from site i to site j is proportional to:

- $\left(\frac{R_0}{R_{i,j}}\right)^6$ due to the dipole-dipole interaction
- $exp\left(-\frac{\epsilon_j-\epsilon_i}{k_BT}\right)$ due to the energy barrier
- the density of states $g(\epsilon_j)$

Obviously there is a competition between two effects:

- For the dipole-dipole interaction term to be large, $R_{i,j}$ should be small.
- However, the energy barrier $\epsilon_j - \epsilon_i$ should also be small; the bigger $R_{i,j}$, the higher the probability to find such a small barrier.

As a result of this competition, the excitation is hopping its way through the energetically and spatially disordered medium, optimizing each hop for R and E. This phenomenon is known as Variable Range Hopping (VRH), first described by Sir Neville Mott [Mot69]. He argued that the diffusion of the particle is determined by the hardest hops it has to pass along its way through the medium. For each jump the exciton makes the number of possible sites it can jump to should be of the order 1, otherwise the hopping process would extinguish after a few hops. The Mott-condition therefore states that the number of possible jumps should be of the order 1

$$\int_{|\vec{R}'|<\vec{R}} d\vec{R}' \int_{E}^{E+\Delta E} g(\varepsilon)d\varepsilon = \mathcal{O}(1), \tag{4.3}$$

For a constant DOS

$$g(\varepsilon) = \begin{cases} \delta^{-1} & \text{for} - \delta/2 \leqslant \varepsilon \leqslant \delta/2, \\ 0 & \text{for} - \delta/2 > \varepsilon > \delta/2. \end{cases} \tag{4.4}$$

(4.3) becomes

$$\alpha R^d \delta \Delta E = 1 \tag{4.5}$$

for a d-dimensional space with α the pre-factor for the volume according to d.

For the optimization of the hopping rates (4.2) is rewritten in the following way:

$$k_0 exp\left[6ln\left(\frac{R_0}{R}\right) - \frac{\Delta E}{k_BT}\right] \tag{4.6}$$

Maximizing the hopping frequency (4.6) for hops upward in energy under the condition (4.5) gives

$$\frac{\partial}{\partial R}\left[6ln\left(\frac{R_0}{R}\right)-\frac{\delta}{\alpha R^d k_B T}\right]=0$$

$$R_{opt}=\left(\frac{d}{6\alpha}\frac{\delta}{k_B T}\right)^{1/d} \tag{4.7}$$

$$\Delta E_{opt}=\frac{6}{d}k_B T \tag{4.8}$$

Note that both R_{opt} and ΔE are independent of the energy level the exciton is jumping from. With (4.2), (4.7) and (4.8) the 'optimal' hopping frequency v_{opt} can be defined as

$$v_{opt}=v_{ij}(R_{opt},\Delta E_{opt})=k_0 R_0^6\left(\frac{de\delta}{6\alpha k_B T}\right)^{-6/d}, \tag{4.9}$$

with $e = 2.7182\cdots$.

Now the temperature dependence of the diffusion coefficient, D, can be evaluated by averaging hopping times of hops upward in energy, $\langle t\rangle$. Hops downward in energy occur exponentially faster than the hops upward in energy. The downward hops can therefore be neglected in the calculation. The average hopping time can be written as

$$\langle t\rangle^{-1}=\langle v_{opt}\rangle_{DOS}=\int_{-\delta/2}^{\delta/2} v_{opt}\times g(\epsilon)d\epsilon \Big/ \int_{-\delta/2}^{\delta/2} g(\epsilon)d\epsilon = v_{opt} \tag{4.10}$$

The diffusion is now determined as [ref Baranovskii et al. PRB62]

$$D\sim R_{opt}^2\langle t\rangle^{-1}=k_0 R_0^6\left(\frac{6\alpha d}{de^{3/2}}\right)^{4/d}\left(\frac{k_B T}{\delta}\right)^{4/d} \tag{4.11}$$

Apparently the temperature dependence of the diffusion of excitations in a constant DOS via the Förster process is algebraic, $T^{4/d}$. This in contrast with the exponential temperature dependence, $\exp\left(-[T_0/T]^{1/(d+1)}\right)$, for diffusion via Abraham-Miller hopping rates as, for instance, charge carriers in doped polymeric systems.

4.3 Exciton Diffusion in a Gaussian DOS - Bässler Hopping

In this section the temperature dependence of exciton diffusion in a Gaussian DOS (4.1) in the high temperature regime, $\sigma/k_B T \ll 1$, is evaluated. Consider an exciton somewhere in the Gaussian distribution at an initial energy E_i, see figure 4.1. We now assume that the exciton is hopping very fast around E_i, within the range $E_{i,min} < E_i < E_{i,max}$. Sometimes it is able to make a hop to the higher energy level E_f, assumed to be the level of critical hops that determine the temperature dependence of the diffusion according to the Mott theory. The temperature regime discussed here is $kT \gg \sigma$. To determine the hopping frequency to E_f the thermal average over E_i is taken

$$v_{total}=\left\langle R^{-6}e^{-\beta(E_f-E_i)}\right\rangle_{th}=R^{-6}e^{-\beta(E_f-E_0)}\left\langle e^{-\beta(E_0-E_i)}\right\rangle_{th}$$
$$\equiv v_{Mott}\times v_{Bässler}, \tag{4.12}$$

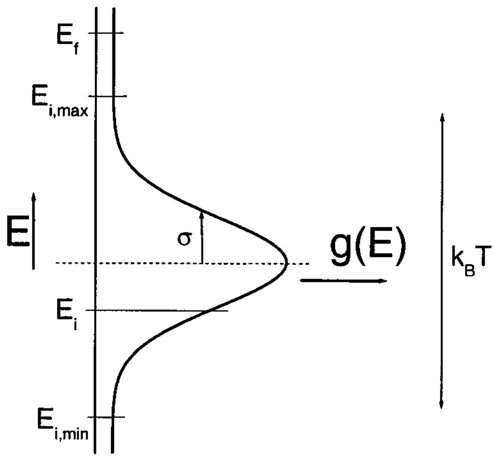

Figure 4.1: The Gaussian density of states.

with $\beta = k_B T$. For mathematical convenience we have assumed an energy level E_0 with $E_{i,min} \leq E_0 \leq E_{i,max}$.
Now we will evaluate the two terms separately in the same temperature regime to determine which one will dominate the temperature dependence. We start with $v_{Bässler}$:

$$\begin{aligned} v_{Bässler} &= \left\langle e^{-\beta(E_0 - E_i)} \right\rangle_{th} \\ &= \int_{E_{i,min}}^{E_{i,max}} e^{-\beta(E_0 - E_i)} \times e^{-\beta E_i} \times g(E_i) dE_i \Bigg/ \int_{E_{i,min}}^{E_{i,max}} e^{-\beta E_i} \times g(E_i) dE_i \end{aligned} \tag{4.13}$$

Our interest is the regime for which $\sigma / k_B T \ll 1$, in the present case this means that $g(E_{i,min}) \approx g(E_{i,max}) \approx 0$. This is represented by $E_{i,min} \to -\infty$ and $E_{i,max} \to \infty$, for which (4.13) becomes

$$v_{Bässler} = e^{-\beta E_0} \int_{-\infty}^{\infty} g(E_i) dE_i \Bigg/ \int_{-\infty}^{\infty} e^{-\beta E_i} g(E_i) dE_i = e^{-\beta E_0} \Bigg/ \left\langle e^{-\beta E_i} \right\rangle_{DOS}, \tag{4.14}$$

with $< f >_{DOS}$ the average of function f over the DOS:

$$\left\langle e^{-\beta E_i} \right\rangle_{DOS} = \frac{1}{\sigma\sqrt{2\pi}} \int_{-\infty}^{\infty} e^{-\beta E_i} e^{-E_i^2/(2\sigma^2)} dE_i \Bigg/ \int_{-\infty}^{\infty} e^{-E_i^2/(2\sigma^2)} dE_i = e^{\frac{1}{2}\beta^2\sigma^2}. \tag{4.15}$$

So finally we write for $v_{Bässler}$

$$v_{Bässler} = e^{-\beta E_0} e^{-\frac{1}{2}\beta^2\sigma^2} \tag{4.16}$$

We evaluate the Mott-term by maximizing v_{Mott} for E_f in the same way as in section 4.2:

$$\begin{aligned} \frac{\partial}{\partial E_f} R^{-6} e^{-\beta(E_f - E_0^*)} &= 0 \\ \frac{\partial R}{\partial E_f} &= -\frac{\beta}{6} R \end{aligned} \tag{4.17}$$

under the Mott-condition (4.3).

$$\begin{aligned} \frac{\partial}{\partial E_f} \left[R^3 \int_{-\infty}^{E_f} g(E)dE = 0 \right] \\ 3\frac{\partial R}{\partial E_f} \int_{-\infty}^{E_f} g(E)dE = -Rg(E_f). \end{aligned} \tag{4.18}$$

Combining (4.17) and (4.18) gives

$$\beta^{-1} = \frac{1}{2g(E_f)} \int_{-\infty}^{E_f} g(\varepsilon)d\varepsilon, \tag{4.19}$$

which defines $E_f = E_f(\beta)$ and $R = R(\beta)$. For v_{Mott} we now write

$$v_{Mott}(E_f) = e^{\beta E_0} \left[\int_{-\infty}^{E_f} g(\varepsilon)d\varepsilon \right]^2 exp \left[-2g(E_f)E_f \Big/ \int_{-\infty}^{E_f} g(\varepsilon)d\varepsilon \right] \tag{4.20}$$

In the high-temperature regime, the same limit as for $v_{Bässler}$ is taken for v_{Mott}

$$\lim_{E_f \to \infty} v_{Mott}(E_f) = e^{\beta E_0}. \tag{4.21}$$

So for the regime of $\sigma \ll k_B T \ll E_f$

$$v_{total} = v_{Mott} v_{Bässler} = e^{-\frac{1}{2}\beta^2\sigma^2}. \tag{4.22}$$

The diffusivity can be written as

$$D \sim e^{-\frac{1}{2}\beta^2\sigma^2}. \tag{4.23}$$

The same temperature dependence was obtained by Huber [Hub83] by using a completely different approach, i.e. the effective medium approach, developed by Movaghar and coworkers, see [Hub83] and references therein. He found for $\sigma/kT \leq 5$ that $D \sim e^{-0.4\beta^2\sigma^2}$.

CHAPTER 5

Monte Carlo Simulations on Polymer and Polymer-Dye Systems

5.1 Introduction

In this chapter the transport properties of excitons in a constant DOS are studied. This gives much information about the general principles of the hopping process. We will also look at the time scales of the relevant processes: τ_{relax}, the time needed for the system to reach thermal equilibrium and $\tau_{pol\to dye}$, the typical time it takes for an exciton to reach a dye molecule. These timescales, together with the lifetime of the exciton τ_{life}, give information under which conditions the capture of the excitons takes place. After that the efficiency of polymer-dye systems is studied.

5.2 Monte Carlo Simulations Technique

The simulations were performed on a cubic lattice consisting of 100x100x100 sites with an inter-site distance a. Their energies were chosen according to the Gaussian probability density (4.1). Periodic boundary conditions were applied to the lattice. The exciton is initially placed in the center of the lattice. A subcell of 15x15x15 sites around the exciton is defined and for each site of this subcell the hopping probability (4.2) is calculated. The parameters used are $k_0 = 300\text{ps}^{-1}$, the inverse lifetime of the excitons, the Förster radius, R_0, which is set to $2a$, with a the lattice constant and the width of the Gaussian distribution $\sigma = 70\text{meV}$. These are the values experimentally found for Polyfluorene [MHOB01]. The normalized probability that an exciton jumps from a site i to any site j within the subcell is

$$P_{ij} = v_{ij} \Big/ \sum_{i \neq j} v_{ij} = v_{ij}\tau, \tag{5.1}$$

with v_{ij} the hopping rate (4.2) and $1/\tau$ the total probability per unit of time for the exciton to jump. Each site in the subcell is given a length according to (5.1) on a 'line' of length 1. A random number from a uniform distribution is chosen that specifies to which site the exciton jumps. The characteristic time τ determines the probability distribution of the waiting time between hops, which is given by

$$P(t) = \frac{1}{\tau} e^{-t/\tau}. \tag{5.2}$$

The time for the jump is determined by choosing a random number from this exponential distribution. This procedure is repeated until the sum of the time increments has reached a fixed value, τ_{sim}. For a polymer system the total number of excitons considered is 1000.

When simulating a polymer-dye system, sites in the bulk are chosen to be dye-sites randomly according to a certain dye fraction. The hopping rate from a polymer-site to a dye-site is identical to the polymer to polymer hopping rate (4.2), i.e. R_0 is the same. The simulation is stopped either after a certain time, τ_{sim}, or when the exciton hops onto a dye-site.

During the simulation, the computer keeps track of the mean position, $\langle R \rangle$, the mean-squared position, $\langle R^2 \rangle$, the mean energy $\langle E \rangle$ and the variance of the energy σ_E as a function of time.

5.3 Relaxation and Diffusion of Excitons in a Constant DOS

In this section we discuss the simulation results of excitons hopping in a constant DOS. The simulations were performed for disorder parameter, δ/k_BT, varying from 0.02 to 150. According to (4.7) the (critical) optimal hopping distance depends on the disorder of the system, see figure 5.4. When R_{opt} decreases and becomes equal to or smaller than 1 lattice constant, the hopping mechanism changes from variable range hoping (VRH) to nearest neighbor hopping (NNH), meaning that there are always a sites adjacent to the exciton it can jump to. For the VRH regime the theory predicts that the temperature dependence of the diffusion is according to the Mott theory as derived in section 4.2. For NNH the hopping process is normally activated.

For a constant DOS (4.4) the equilibrium value of the average energy is

$$\langle \varepsilon \rangle_\infty = \frac{\int\limits_{-\infty}^{\infty} \varepsilon g(\varepsilon) \exp\left[-\frac{\varepsilon}{kT}\right] d\varepsilon}{\int\limits_{-\infty}^{\infty} g(\varepsilon) \exp\left[-\frac{\varepsilon}{kT}\right] d\varepsilon} = k_BT \frac{1 + \frac{1}{2}\frac{\delta}{k_BT} + \left(\frac{1}{2}\frac{\delta}{k_BT} - 1\right) \exp\left[\frac{\delta}{k_BT}\right]}{1 - \exp\left[\frac{\delta}{k_BT}\right]}. \tag{5.3}$$

In figure 5.1 the results of a Monte Carlo simulation visualize the relaxation of excitons for various temperatures. The starting energy is 0 for all temperatures, for $\delta/k_BT = 37.2$ a relaxation started from $E = -0.5\delta$ is also shown. For low values of the disorder-parameter δ/k_BT, the relaxation is complete at $t = 10ps$, whilst for higher disorder it only takes around 100ps for the system to relax. So the relaxation in a constant DOS does not vary much with the temperature.

Looking at the mean-squared displacement in figure 5.2, the relaxation can be divided in two phases. In the first first phase the relaxation is temperature independent and the slope 1 indicates that the motion is regular diffusion. This can be explained by the fact that all excitons for all temperatures start in the middle of the uniform distributed DOS. The number of sites with lower energies in the direct vicinity of each exciton is numerous, hence most of the hops will be nearest neighbor hops.

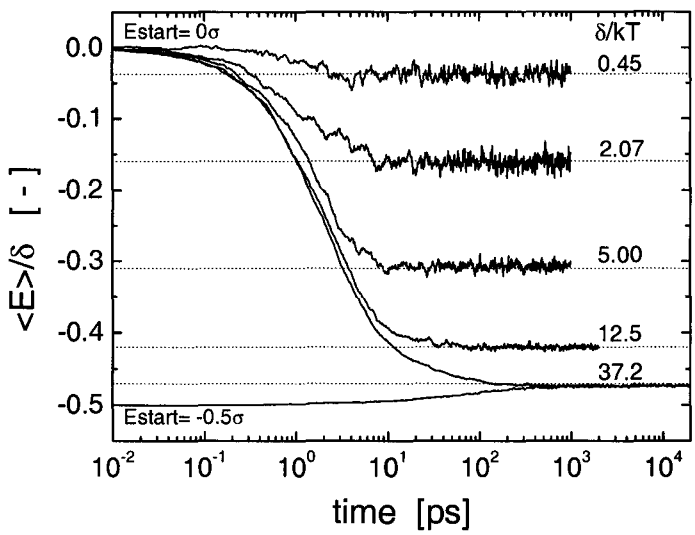

Figure 5.1: Energy relaxation of excitons in a constant DOS. The dotted lines give $\langle\varepsilon\rangle_\infty$ for the various values of δ/k_BT, according to eq.(5.3).

After roughly 1ps, for low temperatures ($\delta/k_BT = 37.2$) the relaxation stalls and the diffusion becomes anomalous. The excitons are in the lower part of the DOS and hops upward in energy are necessary for further relaxation. A new stationary situation is reached at $t = 10^3 ps$, after which the movement of the excitons is again diffusive. Note that the time needed to reach diffusive motion is much longer than the time needed for energetic relaxation. For high temperatures ($\delta/k_BT = 0.45$) there is no second phase, the initial regular diffusion just continues.

For regular diffusion in three dimensions, the diffusivity is given by

$$D = \frac{1}{6}\frac{\langle r^2(t)\rangle}{t}. \tag{5.4}$$

The diffusion constant is calculated for values of the disorder varying from 0.02 to 150. For the high disorder regime (low temperature) D was plotted as a function of (k_BT/δ), as shown in figure 5.3. According to the Mott theory, there should be a linear relation within this regime with slope 4/3 (see section 4.2). Within the range of $\delta/k_BT = 5 - 150$ this linear behavior according to (4.11) was found indeed. By plotting D vs $(k_BT/\delta)^\gamma$ with γ varying from 1 to 2 it was shown that for $\gamma < 4/3$ the curve is superlinear and for $\gamma > 4/3$ the curve is sublinear, thereby confirming the validity of the Mott theory.

In the present simulations the crossover from VRH to NNH is found for $\delta/k_BT \leq 5$. For NNH the hopping process is normally activated, therefore the temperature dependence of the diffusion coefficient is $D \propto \exp(T_0/T)$. In figure 5.5 log(D) vs δ/k_BT is plotted for $\delta/k_BT \leq 5$, the linear behavior is evident.

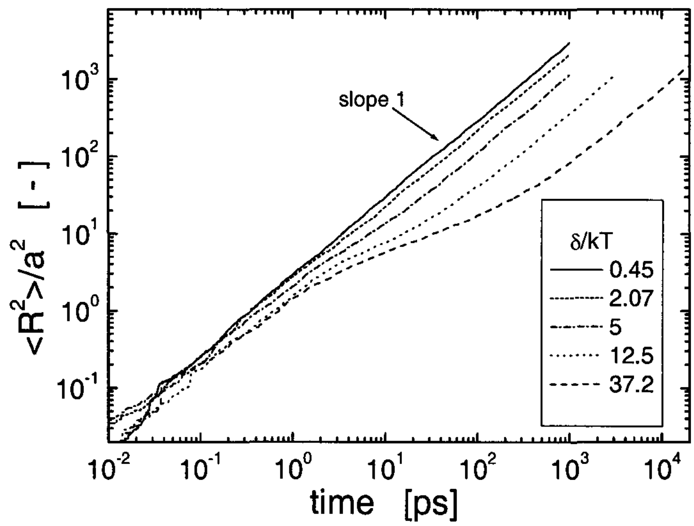

Figure 5.2: Mean-squared distance of excitons in a constant DOS.

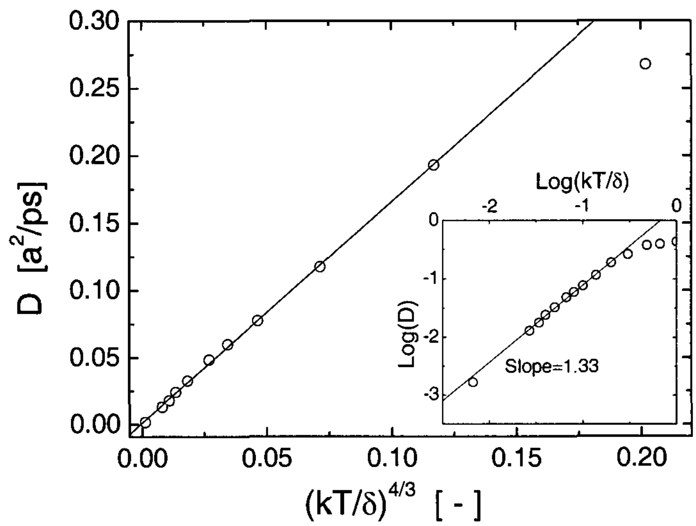

Figure 5.3: Temperature depedence of the diffusivity of excitons in a constant DOS.

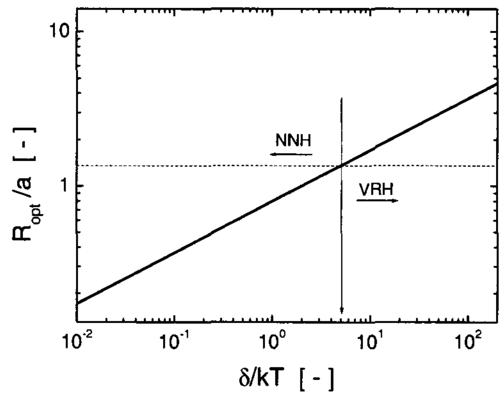

Figure 5.4: The critical hopping distance (4.7) of excitons in a constant DOS as a function of T^{-1}. The arrow indicates the point at which a crossover from NNH to VRH was found in the simulations.

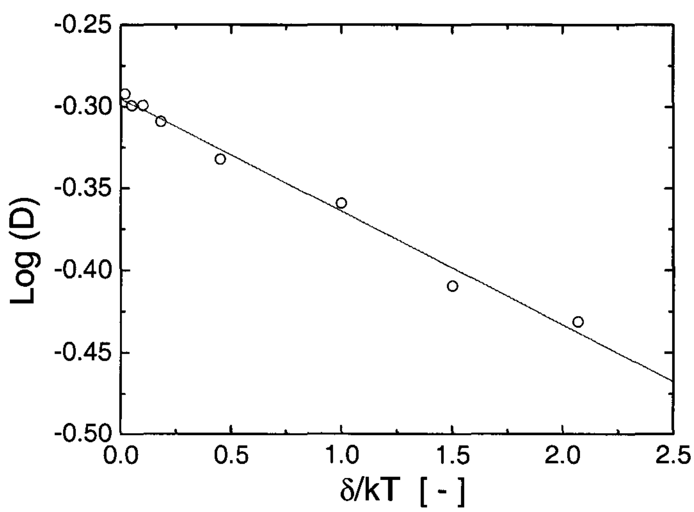

Figure 5.5: Normal activated (Arrhenius) behavior of excitons in a constant DOS.

5.3.1 Conclusions

In this section we have shown that for Försterprocesses the Mott theory is applicable. This can be concluded from the temperature dependence of de diffusivity, see figure 5.3. The crossover from VRH to NNH at low disorder was shown to be a crossover from Mott hopping to normal activated hopping. This crossover is characterized by the optimal hopping distance, i.e. for $R_{opt} \lessapprox 1$ ($\delta/k_BT \leq 5$) the process is NNH, for $R_{opt} \gtrapprox 1$ ($\delta/k_BT > 5$) VRH.

5.4 Relaxation and Diffusion of Excitons in a Gaussian DOS

As mentioned before, from the literature it is known that excitons in disordered media like polymers experience a Gaussian DOS. From the energy relaxation we can define a typical relaxation time, τ_{relax}, for the system to reach thermal equilibrium. Later in this report we will compare this parameter with other timescales.

In this section we present Monte Carlo simulations of excitons in such a DOS. In figure 5.6 the average energy as a function of time shows relaxation towards the thermal equilibrium, which, together with (4.1), can be described as

$$\langle E \rangle_\infty = \frac{\int\limits_{-\infty}^{\infty} \varepsilon g(\varepsilon) \exp\left[-\frac{\varepsilon}{kT}\right] d\varepsilon}{\int\limits_{-\infty}^{\infty} g(\varepsilon) \exp\left[-\frac{\varepsilon}{kT}\right] d\varepsilon} = -\frac{\sigma^2}{k_B T}. \tag{5.5}$$

The standard deviation of an ensemble in thermal equilibrium is given by

$$\sigma_\infty{}^2 = \left\langle E^2 \right\rangle_\infty - \langle E \rangle_\infty^2 = \sigma^2. \tag{5.6}$$

The excitons all started their relaxation at the same energy, $E_s = 0\sigma$. For one simulation (at 500K) the the starting energies of the excitons were chosen from an equilibrium distribution according to (5.5) and (5.6). For high temperatures the system is able to relax within a reasonable time as shown in figure 5.6 and 5.8. At the same time that $\langle E \rangle$ reaches its value for thermal equilibrium, $\langle E \rangle_\infty$, the width of the energy distribution, σ_E reaches the value 1. From figure 5.6 we would like to deduce the characteristic relaxation times, τ_{relax}. However, it is obvious that the energy relaxation is far from exponential in time which makes it difficult to define a 'regular' time constant. Here we define τ_{relax} as the time at which $\langle E \rangle$ has reached 95% of its final equilibrium value, $\langle E \rangle_\infty$. The values are plotted in figure 5.19 and evaluated in Section 5.8.

The width of the energy distribution, σ_E, shows some interesting dynamics (cf. figure 5.8). Since all excitons start in the middle of the DOS there are enough sites with lower energy available, i.e. the initial relaxation is temperature independent and σ_E increases monotonic. After this initial effect, there is an decrease of σ_E for $T = 300$K, indicating that the system cannot relax on short time scales (this is also characterised by the transition from regular to anomalous diffusion, cf. Figure 5.9). For longer times σ_E increases again toward σ_∞. In figure 5.7 we show the evolution of the spectrum at 300K. For short times (0.1ps) most of the excitons are at the starting energy, denoted by a 'delta peak' at 0σ. For longer times the maximum of the spectrum shifts to lower energies while the width of the spectrum increases, as was shown in figures 5.6 and 5.8. One can even observe the temporal decrease of the width at 10ps. The spectra are normalized by the number of excitons present in the system.

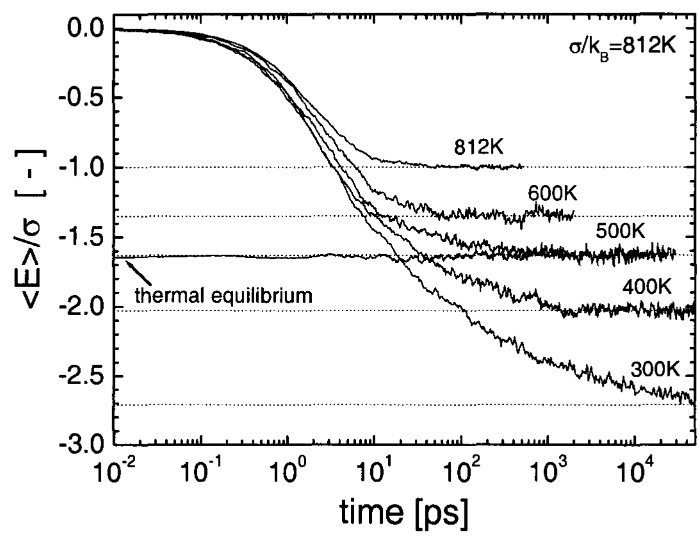

Figure 5.6: Energy relaxation of excitons in a Gaussian DOS. The dotted lines are the values of the thermal equilibrium according to 5.5

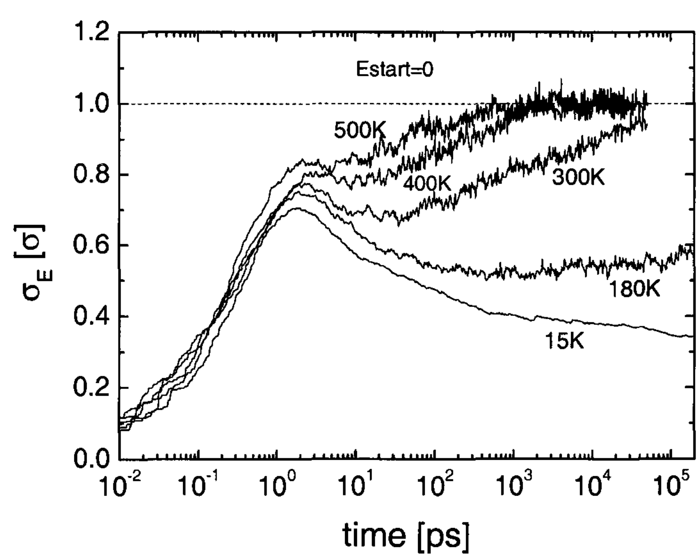

Figure 5.7: Width of the energy distribution of an ensemble of excitons.

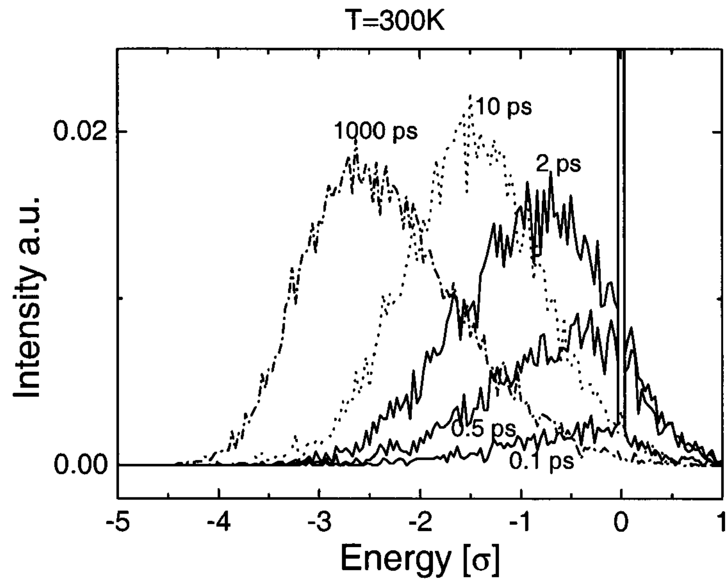

Figure 5.8: Evolution of the spectrum of excitons at 300K.

From the time-dependent mean-squared distance (cf. figure 5.9) we learn that the initial relaxation is also temperature-independent (normal) diffusion, followed by a region of anomalous diffusion until regular diffusion sets in again. In figure 5.10 the logarithm of the diffusion coefficients for different temperatures are set out against T^{-2}. For $(\sigma/kT)^2 < 7.33$ or $\sigma/kT < 2.7$ we see the regime in which Bässler-hopping dominates, described in section 4.3, which is in good agreement with the findings of Huber [Hub83]. He also reported for low temperatures ($\sigma/kT > 5$) a crossover from the $(1/T)^2$ behavior to an activated $(1/T)$ law. Because of the long simulation times for low temperatures we could not generate enough data to verify this.

Finally, we note that if one uses a cut-off Gaussian distribution (the cut-off represents, for example, the Fermi energy in a many particle system) that for low enough temperatures the distribution resembles that of a constant distribution (cf. section 4.2). So for this regime there should be a crossover to the (Mott) temperature dependence of the constant DOS, i.e. equation (4.11).

5.4.1 Conclusions

It is shown that for exciton transport in a Gaussian DOS, for high temperatures the system is able to relax towards a thermal equilibrium within the time limits of our simulations. A definition of the relaxation time was formulated and determined accordingly. The high-temperature dependence of the diffusivity found from the simulations is as described in section 4.3 and is comparable with results found in the literature.

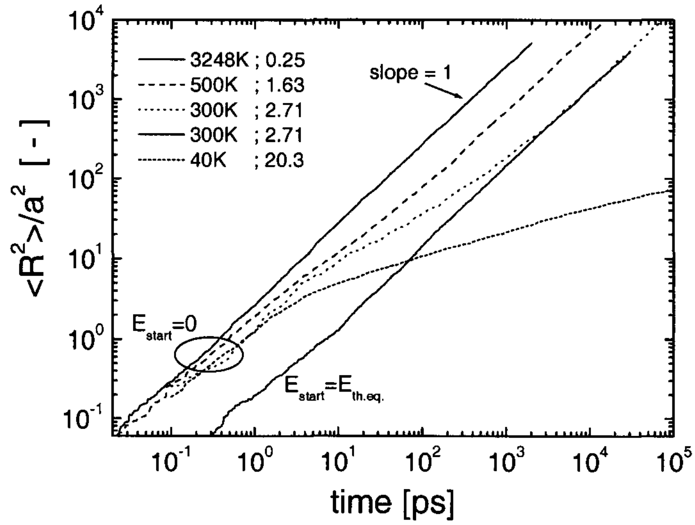

Figure 5.9: Mean squared distance of excitons in a Gaussian DOS.

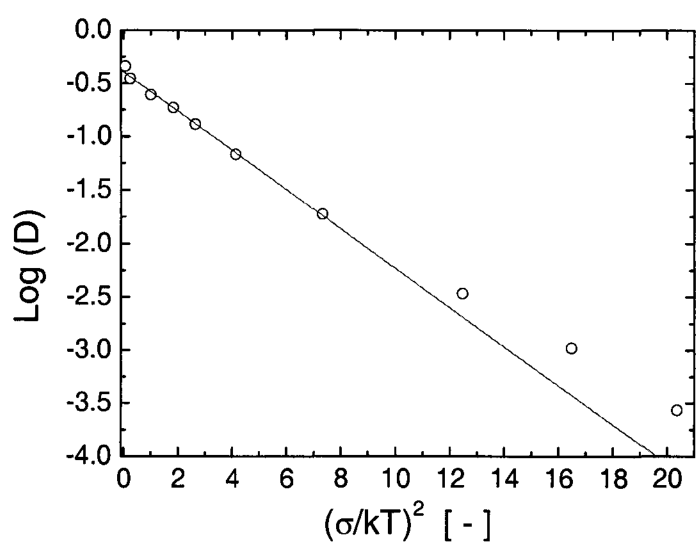

Figure 5.10: Temperature depedence of the diffusion coefficient of excitons in a Gaussian DOS in the high-temperature regime.

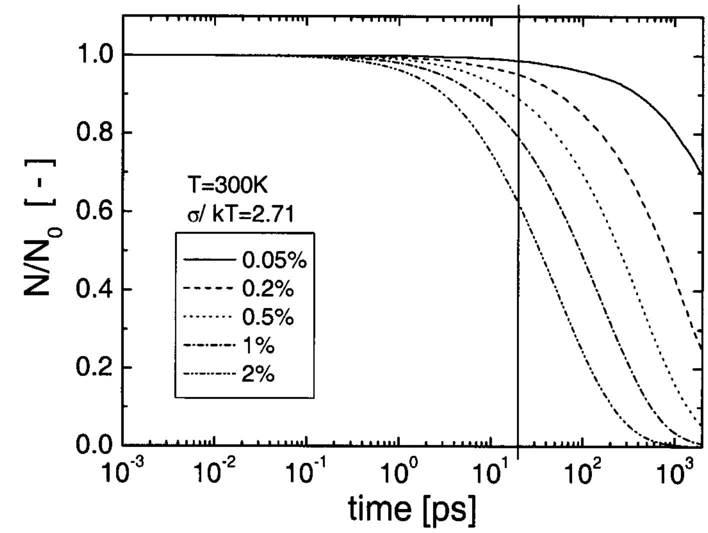

Figure 5.11: Fraction of excitons left as a function of time for different percentages of dye molecules. N_0 is the number of excitons in the ensemble at $t = 0ps$

5.5 Influence of Dye-Doping on Transport Exciton Properties

In this section we will see what the influence of dye-doping is on the transport properties of excitons moving in a system with a Gaussian DOS.

In figure 5.12 the time dependence of the average energy is shown for various percentages of dye molecules. For low dye concentrations (0.05%) the relaxation does not differ much from the relaxation of an all-polymer system (figure 5.6). For higher concentrations one observes, after approximately 20ps, a shift towards lower energies (red shift) for increasing fractions of dye. The high-energy excitons are more mobile and therefore mainly captured by the dye molecules leaving the low-energy excitons in the bulk. Taking out the excitons of high energy (i.e. above average energy) would result in a smaller energy distribution. However, according to figure 5.13 the width of the energy distribution is not (noticeably) disturbed by the exciton capture. A possible explanation is that the distribution is not Gaussian and that the shape of the distribution, at a certain time, can change while the width, determined as ${\sigma_E}^2 = \langle E^2 \rangle - \langle E \rangle^2$, remains constant. This can be seen in figure 5.14 where the spectrum for three different concentrations is plotted at $t_1 = 50$ps and at $t_2 = 400$ps. At $t = t_1$ we see no effect due to the dye, all curves overlap. However, for $t = t_2$ we see a distinct influence of the dye: the maximum of the spectrum ($= \langle E \rangle$) shifts to lower energies while the width of the spectrum becomes asymmetrical. The intensities of the spectra are also normalized according to the number of excitons still present in the system.

The average energy is affected by the dye for all concentrations beyond the same characteristic time ($t \approx 20ps$). However, the fraction of excitons captured before this is substantial (see Figure 5.11). The time at which this capture becomes noticeable depends on the dye

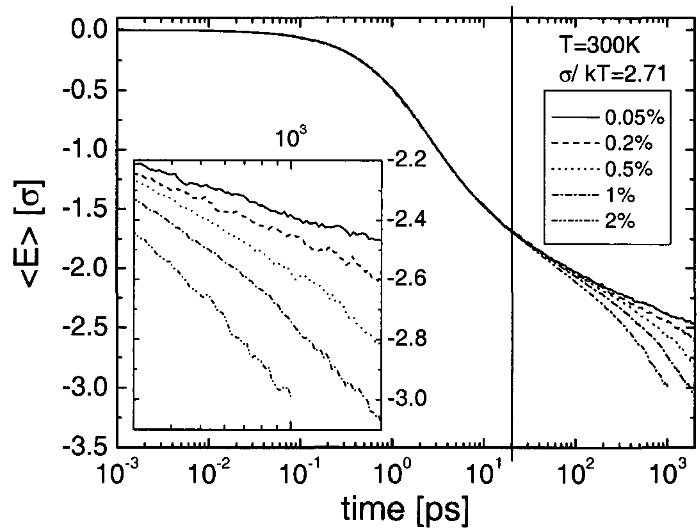

Figure 5.12: Influence of the presence of dye molecules on the average energy. The curve of 2% dye was cut off after 1000ps, for longer times the number of excitons present in the system was not sufficient for decent statistics.

concentration and shifts towards shorter times for higher concentrations of dye. Since the capture of excitons for $t < 20$ps has no effect on $\langle E \rangle$ we can conclude that this capture is independent of the energy.

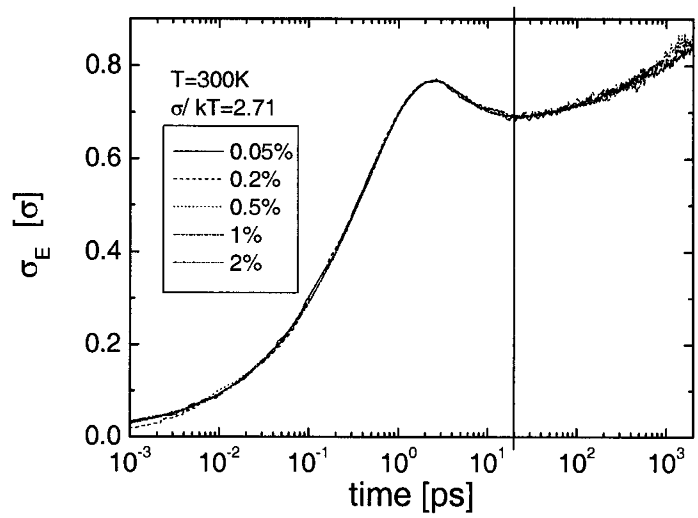

Figure 5.13: Influence of the presence of dye molecules on the variance of the energy.

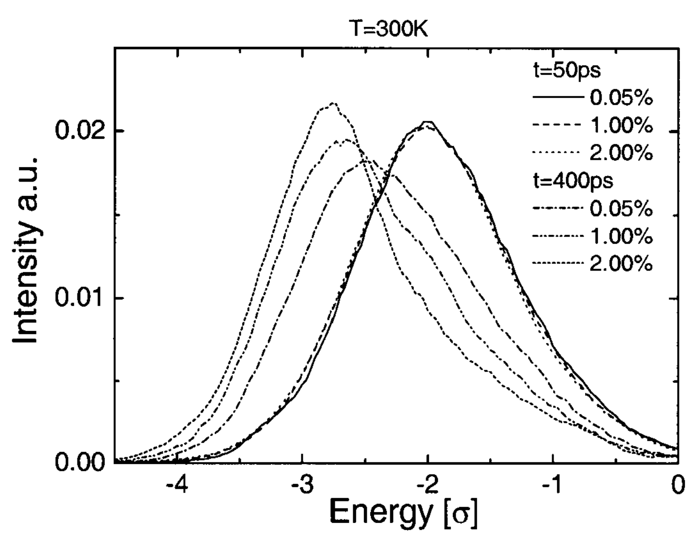

Figure 5.14: Spectrum of the exciton energy in a dye-doped system at 50ps and 400ps.

5.6 Concentration Dependence of the Exciton Capture Rate - Diffusion-Controlled Reactions

When dye molecules are dispersed in the polymer they can act as a trapping center for the excitons. In this section we study the capture rate of the excitons by the dye as a function of temperature and dye concentration, using the theory of diffusion-controlled reactions. From this capture rate we determine the last time constant, $\tau_{pol \to dye}$, the typical time for an exciton to reach a dye molecule.

The theory of diffusion-controlled reactions was first formulated by Smoluchowski [FD76]. The basic idea is that the rate of a reaction is be dominated by slow diffusive motion for the reacting partners to approach each other, followed by instantaneous reaction. The system consists of three parts denoted as fluid, particles and sinks. The fluid serves merely as an inert solvent in which particles carry out diffusive motion. A particle and a sink can react and after reaction the particle disappears from the system. The change of the sink as a result of the reaction is neglected. The sinks are taken to be completely at rest and to have a radius R. In our case the fluid is represented by the polymer bulk, the particles by the excitons and the sinks by the dye molecules.

In a dilute system it suffices to consider a single pair of reactants, competition for excitons between dye molecules can be neglected. Thus the particle number density $n(\mathbf{r}, t)$ satisfies the diffusion equation

$$\frac{\partial n}{\partial t} = D_0 \nabla^2 n \tag{5.7}$$

in the part of space occupied by the fluid. One assumes that a particle diffusing towards a sink is absorbed instantaneously upon contact. This is expressed by the boundary condition that the particle density is vanished at the surface. In the steady-state situation, the equation to be solved is

$$\nabla^2 n = 0, \tag{5.8}$$

with the boundary condition

$$n(\mathbf{r}) = 0 \text{ at } r = R, \tag{5.9}$$

where R is the radius of the sink whose center is taken to be at the origin. For uniform density n_0 at infinity the solution is

$$n(\mathbf{r}) = n_0 \left(1 - \frac{R}{r}\right) \tag{5.10}$$

The particle current density is given by

$$\mathbf{j} = -D_0 \nabla n \tag{5.11}$$

and integrating over the surface of the sink one finds the number of particles absorbed per second

$$J = 4\pi D_0 R n_0. \tag{5.12}$$

On a macroscopic scale the equation for the average particle density $N = \langle n \rangle$ therefore becomes

$T[K]$	$\mu[ps^{-1}]$	$D[a^2ps^{-1}]$	$R[a]$
812	$6.3 * 10^{-4}$	0.2480	0.40
500	$4.3 * 10^{-4}$	0.1310	0.52
400	$2.7 * 10^{-4}$	0.0685	0.63
300	$0.9 * 10^{-4}$	0.0187	0.76

Table 5.1: Calculated values of R for various temperatures.

$$\frac{\partial N}{\partial t} = D_0 \nabla^2 N - k_0 \rho N \tag{5.13}$$

with rate constant $k_0 = 4\pi D_0 R$ and sink number density ρ.

If we only look at the capture of excitons by the dye molecules we can write the capture rate of excitons in a dye-doped polymer as

$$\mu = \frac{N(t) - N(t + \Delta t)}{\overline{N}\Delta t} \approx -\frac{1}{N}\frac{\partial N}{\partial t} = 4\pi D_0 \rho R, \tag{5.14}$$

with $\Delta t = 20ps$ and $\overline{N}$ the time-average number of excitons left in the system between t and $t + \Delta t$. From (5.14) we see that μ scales linearly with the dye density ρ.

In figure 5.15 μ is plotted for 15K and 500K. For $T = 15K$ μ is not constant in time due to the fact that the system is far from equilibrium so the motion is not diffusive, see figure 5.9. For $T =$ 500K we see from figure 5.9 that starting from $t =$ 100ps a diffusion coefficient can be defined and the theory described above is applicable. Figure 5.15 (a) and (c) show μ for 15K and 500K respectively for different dye concentrations, (b) and (d) are the data scaled to their dye concentration onto a mastercurve (5.14).

In table 5.1 some values of R are calculated for different temperatures, for μ we used the values corresponding to the master curve. We see that R is typically smaller than a, the lattice constant. This is what can be expected, since the boundary condition (5.9) states that the particle density vanishes at $\mathbf{r} = R$. In our simulations the exciton can exist on neighboring sites of a dye molecule, therefore R should be smaller than the intersite distance.

The time constant $\tau_{pol \to dye}$ follows directly from μ:

$$\tau_{pol \to dye} = \mu^{-1}, \tag{5.15}$$

and will be evaluated in section 5.8.

The assumption that the particle density tends to a constant at large distance from a single sink is of key importance. For higher concentrations this condition does not hold anymore, the excitons will be able to "see" two or more dye molecules at the same time. For this case Felderhof *et al.* have set up a theory describing the concentration dependence of the caption rate of a diffusion-controlled reaction [FD76].

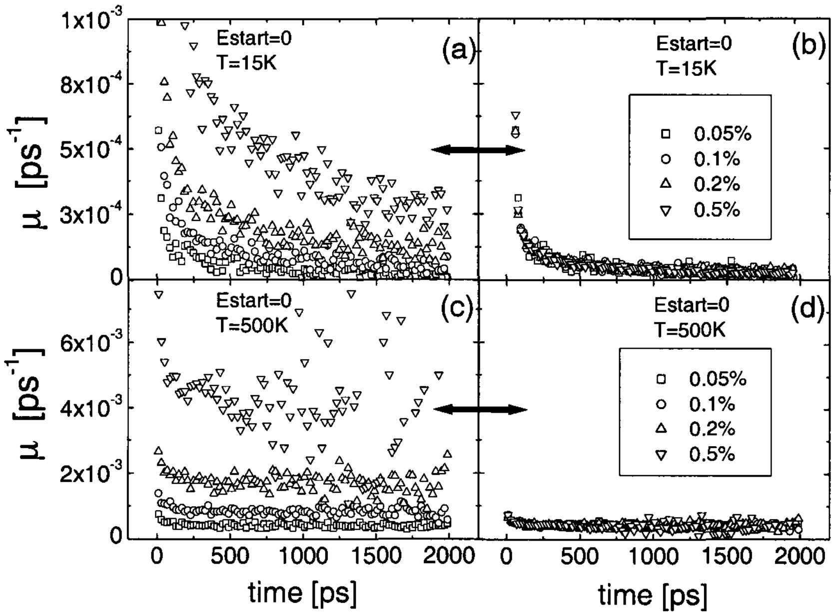

Figure 5.15: Capture rate of excitons on dye molecules, (b) and (d) are linearly scaled according to the concentrations of dye.

5.7 Efficiency of Polymer-Dye Systems

To define the efficiency of a system we look at the fraction of excitons that is captured by dye molecules after 2ns. There are two mechanisms that terminate an exciton:

- the natural lifetime of the exciton,
- capture of the exciton by a dye molecule.

The system parameters used in this study are those of polyfluorene. The average lifetime, τ_{life}, of excitons in polyfluorene is found to be 300ps [ref. Stefan]. The simulations are now performed in the same way as described in section 5.2, only for each run the simulation time, τ_{sim}, is now chosen from an exponential distribution

$$P(t)dt = e^{-t/300}dt. \tag{5.16}$$

If τ_{sim} exceeds 2ns then it is set to 2ns. During the simulation two things can happen. Either the exciton is captured by a dye molecule or it 'decays' after τ_{sim}, either way the simulation is stopped. The fraction of excitons that is captured by dye molecules is said to be the efficiency.

In the present study two kinds of simulations were performed:

- Photoluminescence simulations
- Electroluminescence simulations

The main difference is that in photoluminescence excitons are formed in the polymer at a single energy level (in our simulations denoted as E_{start} or E_s).
In electroluminescence we assume that the excitons are formed throughout the entire bulk, independent of the energy of the site. The energies of the sites are distributed according to a Gaussian, therefore the starting energies of the excitons is distributed according to the same Gaussian.

5.7.1 Photoluminescence

The total number of runs/excitons for one simulation is 10,000. Each run was started at the same energy. As shown in sections 5.4 and 5.5 there are three parameters that determine the dynamics of the excitons:

1. the disorder parameter, σ/k_BT,
2. the starting energy of the excitons, E_s,
3. the concentration of dye molecules.

The influence of all three parameters is shown in figure 5.16. If we look at the curves of 0.5%, we see for the low starting energies ($E_s = -3, -4, -4.5\sigma$) that there is a threshold temperature ($\approx 300K$) above which the efficiency increases rapidly. Below this temperature there is simply not enough (thermal) energy available for jumps upward in energy and the mobility of the excitons is low. This threshold temperature decreases for higher starting energies. The difference in efficiency for all starting energies is fairly small and constant at low temperatures, from 100K the difference becomes more pronounced and almost vanishes again at 812K, at this point $\sigma/k_BT = 1$ so the exciton can jump anywhere in the Gaussian.
For lower concentrations (0.1%) the difference between low and high starting energies disappears. The threshold temperature is now more or less constant for all starting energies ($\approx 200 - 300K$).

Plotting the efficiency as a function of concentration as done in figure 5.17 reveals interesting features. For low temperatures ($T \leq 200K$) the efficiency scales linearly with the concentration. For higher temperatures the dependence is sublinear. This can be explained by the fact that for low temperatures the exciton only makes a few hops within its lifetime. The probability of hopping onto a dye molecules is direct proportional to the number of dye molecules present in the system. For higher temperatures the excitons make many jumps and have therefore a higher probability of encountering a dye molecule, less dependent on the concentration.

5.7.2 Electroluminescence

The number of runs/excitons per simulation in the case of electroluminescence is 20,000. The starting energy of the excitons is now according to (4.1), the same distribution as the sites . The number of parameters that governs the dynamics is now reduced to two:

1. the disorder parameter, σ/k_BT,
2. the concentration of dye molecules.

In figure 5.18 the efficiency as a function of the two parameters is plotted. The behavior is similar to that of the photoluminescence efficiency as can be seen in figure 5.18.

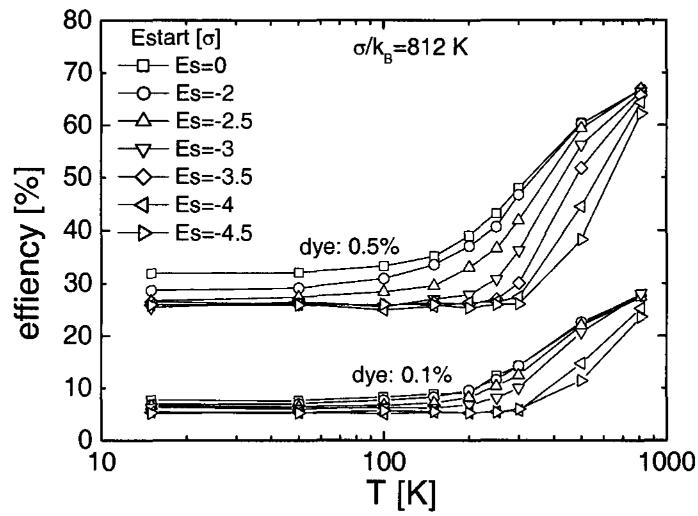

Figure 5.16: Efficiency vs temperature of polymer-dye systems as a function of dye concentration.

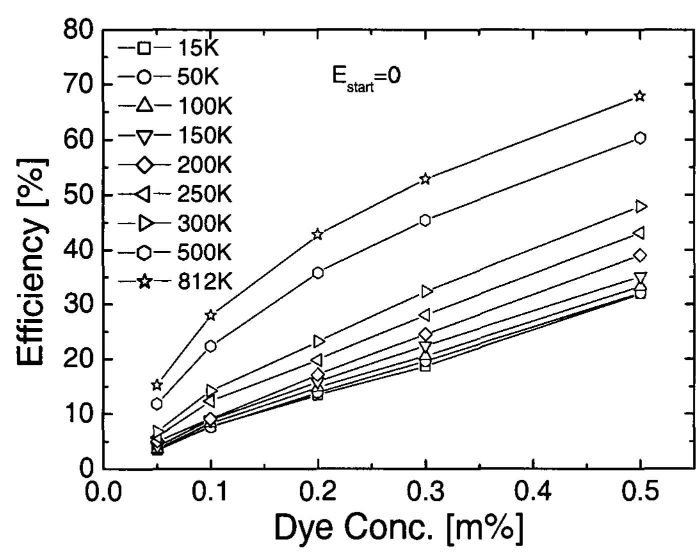

Figure 5.17: Efficiency vs dye concentration of a polymer-dye system as a function of the temperature.

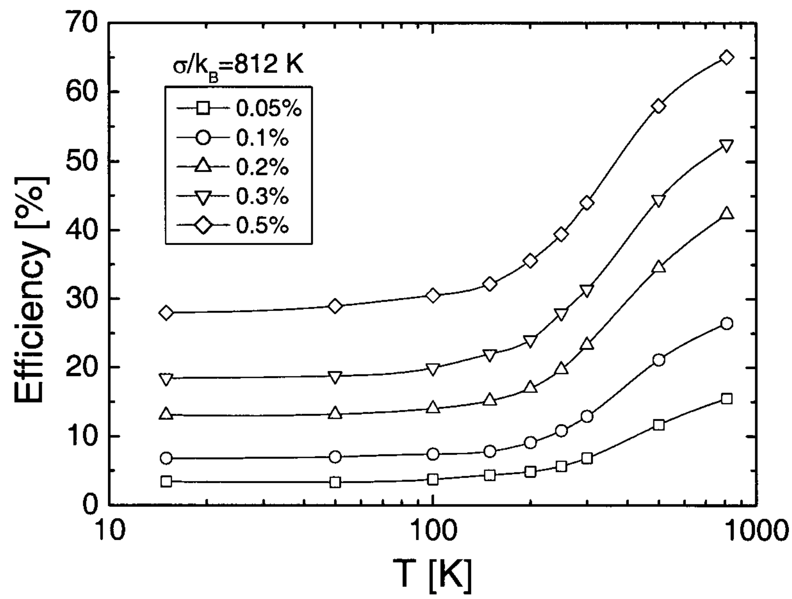

Figure 5.18: Efficiency of polymer-dye systems. The solid lines are guides to the eye.

5.8 Comparison of Time Constants

We can now compare the different time constants as defined in section 5.4 (τ_{relax}) and 5.6 ($\tau_{pol\to dye}$), see figure 5.19. Although the time constants $\tau_{pol\to dye}$ are obtained from the data of PL simulations (a single starting energy for all excitons) they are also characteristic for EL simulations since they represent a characteristic capture time of a system in thermal equilibrium irrespective of the starting conditions of the experiment.

We can divide figure 5.19 into two temperature regimes:

- T <420K: In this regime $\tau_{relax}>$ $\tau_{pol\to dye}>$ τ_{life}. The system is not in thermal equilibrium and because $\tau_{pol\to dye}>$ τ_{life} one would expect that only a small fraction of the excitons is able to reach a dye molecule.

- T >420K: In this regime τ_{relax} < $\tau_{pol\to dye}<$ τ_{life}. The system is able to relax towards thermal equilibrium within the lifetime of the excitons and since $\tau_{pol\to dye}$ < τ_{life} one would expect high efficiencies.

What might seem strange is that even though at 300K $\tau_{pol\to dye} \gg \tau_{life}$ the efficiency is over 40% for both EL and PL experiments. This can readily be explained by the fact that $\tau_{pol\to dye}$ is determined when the system is in thermodynamic equilibrium, before this equilibrium is reached $\tau_{pol\to dye}$ is a function of time and is much smaller than the stationary value (cf. figure 5.15(b), and bare in mind that $\tau_{pol\to dye} = \mu^{-1}$). Apparently most of the excitons are captured by the dye molecules under non-equilibrium conditions.

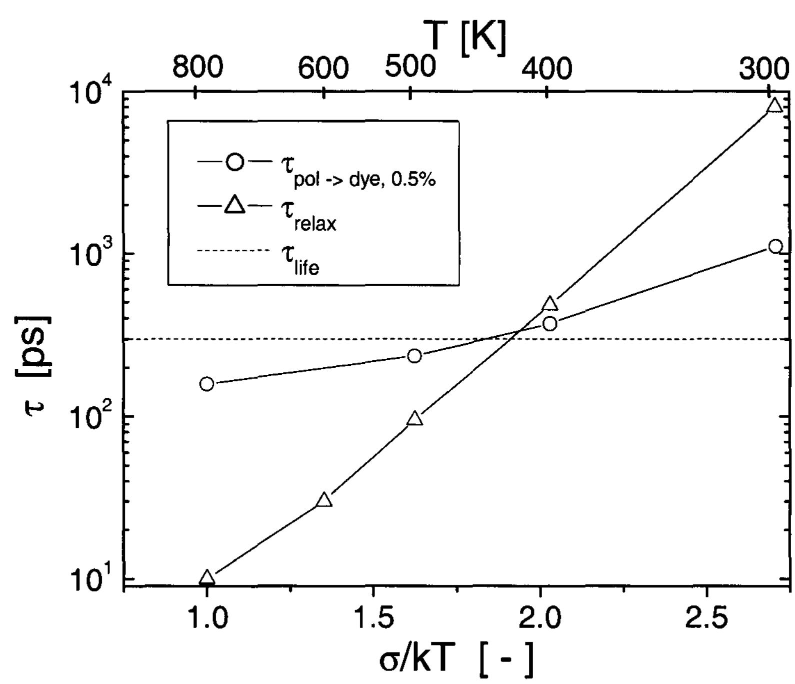

Figure 5.19: Comparison of time constants. The time constants are all obtained from systems with a Gaussian DOS.

CHAPTER 6

Conclusions and Recommendations

6.1 Conclusions on the Dynamics of Excitons in Polymer and Polymer-Dye Systems

- An analytical expression of the temperature dependence of the diffusivity of excitons in a constant DOS is derived using the Mott theory. The validity of this expression was shown by Monte Carlo (MC) simulations. Also a crossover from Mott-hopping (variable range hopping) to normal activated behavior (nearest neighbor hopping) is shown by MC simulations.

- An analytical expression for the temperature dependence of the diffusion coefficient of excitons in a Gaussian DOS is derived and experimentally confirmed by MC simulations.

- The average energy of the excitons in the polymer shifts to lower values (red shift) upon molecular doping.

- The capture rate of excitons by dye molecules in polymer-dye systems scales linear with the dye concentration.

- High efficiencies (30%-70%) of polymer-dye systems were found for fairly low dye concentrations (0.5%) for both photoluminescence and electroluminescence simulations

- The efficiency of polymer-dye systems is mostly determined by the capture of excitons by dye molecules under non-equilibrium conditions.

6.1.1 recommendations

The shift in average energy upon dye-doping was found under non-equilibrium conditions. I would be interesting to see what the behavior is under equilibrium conditions. This means that the simulation time should be increased or the temperature should be increased. Also real photoluminescence experiments can be done on dye-doped polymer systems to see if the red shift experimentally can be observed.

6.2 Conclusions on the Charge-Carrier Dynamics

- Upon molecular doping the change in compensation voltage (V_0) in double-carrier devices is measured by two independent methods, i.e. photovoltaic measurements and resistance measurements.

- The change in compensation voltage (V_0) in double-carrier devices upon molecular doping is due to modification of the polymer-cathode interface. The work function of the cathode plays a crucial role, only devices with low work function cathodes (electron injectors) show a change in V_0.

- By adding molecular dopants the $C(V)$ characteristics of a double-carrier device tend to those of a hole-only device. This is an indication that the dye acts as a trap for electrons.

- Hole mobilities derived from the negative differential ($-\Delta B$) curves from hole-only and double-carrier devices have different field dependencies. The values of μ_0 and γ of the hole-only device are in good agreement with the values generally found in the literature. This can be explained by the fact that in the double-carrier device electrons are present in the bulk, which changes the field distribution. Also recombination could play a role in the change of the mobility.
  Another possibility is that it is an artefact of the method of determining $-\Delta B$, i.e. $C(V_{built-in})$ is not a good reference.

- The negative differential susceptance of a double-carrier device shows narrowing of the electron peak upon doping, which is also an indication of electron trapping. No significant effect is seen on the width of the hole peak.

- The hole mobility of holes in hole-only devices is not affected by molecular doping.

- The hole mobility of holes in double-carrier devices is affected by molecular doping. The values of μ_0 and γ tend to those of hole-only devices for high doping concentrations.

6.2.1 recommendations

In the negative differential plots of dye-doped PLEDs two relaxation peaks are visible. One of them (the electron peak) is, for low bias, only half visible due to the fact that the impedance analyzer is not able to measure below 20Hz. It would be recommended to either adjust the experimental setup to be able to measure at lower frequencies or to increase the temperature during the measurements. The latter causes a shift of the relaxation peak to higher frequencies.

APPENDIX A

Hole Mobility DC Dye

Recent measurements indicate other built-in potentials than mentioned in section 3.3. A built-in potential of 1.95V for a double-carrier device without dye was measured. Assuming the same dependence of the built-in potential on the dye concentration as measured in section 3.3, the hole mobilities as a function of dye concentration are as shown in figure A.1. The field dependence, γ, changes more for increasing dye. The the zero-field mobility, μ_0, and the field dependence, γ, for 2.5% are very close to the values of an hole-only device (figure 3.17).

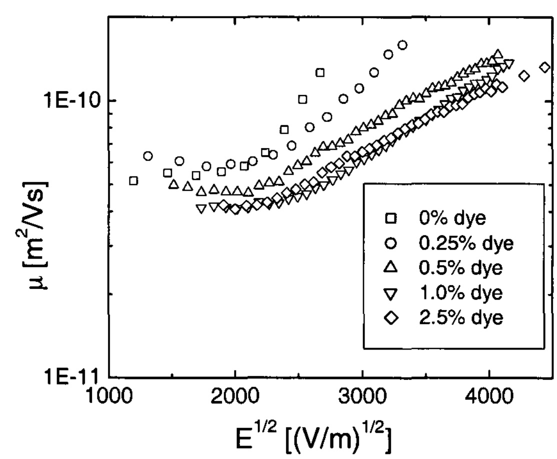

Figure A.1: Mobility of holes in a double-carrier device as a function of dye concentration. The values of $V_{built-in}$ used for this plot are similar to those presented in figure 3.5 increased with 0.25V

However, the author wishes to stress that the measurement results as presented in section 3.3 are most likely to be true and that this Appendix is added solely to give a complete overview of the work done so far.

BIBLIOGRAPHY

[BB85] H. Böttger and V.V. Bryksin, *Hopping conduction in solids*, Akademie-Verlag Berlin, 1985.

[Bec00] H. Becker, Adv. Mater. **12** (2000), 42.

[BV00] P.W.M. Blom and M.C.J.M Vissenberg, *Charge transport in poly(p-phenylene vinylene) light-emitting diodes*, Materials Science and Engineering **27** (2000), 53–94.

[Dex53] D.L. Dexter, *A theory of sensitized luminescence in solids*, Journal of Chemical Physics **21** (1953), no. 5, 836–850.

[FD76] B.U. Felderhof and J.M. Deutch, *Concentration dependence of the rate of diffusion-controlled reactions*, The Journal of Chemical Physics **64** (1976), no. 11, 4551–4558.

[Hub83] D.L. Huber, *Diffusion of optical excitation at finite temperatures*, Journal of Chemical Physics **78** (1983), no. 5, 2530–2532.

[LM70] Murray A. Lampert and Peter Mark, *Current injection in solids*, Academic Press, New York and London, 1970.

[MBP99] H.C.F. Martens, H.B. Brom, and P.W.Blom, *Frequency-dependent electrical response of holes in poly(p-phenylene vinylene)*, Physical Review B **60** (1999), no. 12, R8489–R8492.

[MHB00] H.C.F. Martens, J.N. Huiberts, and P.W. Blom, *Simultaneous measurements of electron and hole mobilities in polymer light-emitting diodes*, Applied Physics Letters **77** (2000), no. 12, 1852–1854.

[MHOB01] Stefan C.J. Meskers, Jens Hübner, Michael Oestreich, and Heinz Bässler, *Dispersion relaxation dynamics of photoexcitations in a polyfluorene film involving energy transfer: experiment an monte carlo simulations*, Journal of Chemistry B **105** (2001), no. 38, 9139–9149.

[Mot69] N.F. Mott, Phil. Mag. **19** (1969), 835.

[MPB+01] H.C.F. Martens, W.F. Pasveer, H.B. Brom, J.N. Huiberts, and P.W.Blom, *Crossover from space-charge limited to recombination limited transport in polymer light-emitting diodes*, Physical Review B **63** (2001), 125328.

[MSBS98] G.G. Malliaras, J.R. Salem, P.J. Brock, and J.C. Scott, *Photovoltaic measurements of the built-in potential in light emitting diodes and photodiodes*, Journal of Applied Physics **84** (1998), no. 3, 1583–1587.

[SSKP02] William R. Salaneck, Kazuhiko Seki, Antoine Kahn, and Jean-Jacques Pireaux, *Conjugated polymer and molecular interfaces: Science and technology for photonic and optoelectronic applications*, Marcel Dekker, 2002.